Stochastic Time-Optimal Trajectory Planning for Connected and Automated Vehicles in Mixed-Traffic Merging Scenarios

Viet-Anh Le, *Student Member, IEEE*, Behdad Chalaki, *Member, IEEE*, Filippos N. Tzortzoglou, *Student Member, IEEE*, and Andreas A. Malikopoulos, *Senior Member, IEEE*

***Abstract*— Addressing safe and efficient interaction between connected and autonomous vehicles (CAVs) and human-driven vehicles (HDVs) in a mixed-traffic environment has attracted considerable attention. In this article, we develop a framework for stochastic time-optimal trajectory planning for coordinating multiple CAVs in mixed-traffic merging scenarios. We present a data-driven model, combining Newell's car-following model with Bayesian linear regression (BLR), for efficiently learning the driving behavior of human drivers online. Using the prediction model and uncertainty quantification, a stochastic time-optimal control problem is formulated to find robust trajectories for CAVs. We also integrate a replanning mechanism that determines when deriving new trajectories for CAVs is needed based on the accuracy of the BLR predictions. Finally, we demonstrate the performance of our proposed framework using a realistic simulation environment.**

***Index Terms*— Bayesian linear regression (BLR), connected and autonomous vehicles (CAVs), mixed traffic, stochastic control, trajectory planning.**

I. Introduction

A. Motivation

THE advancements in connectivity and automation for vehicles present an intriguing opportunity to reduce energy consumption, greenhouse gas emissions, and travel delays while still ensuring safety requirements. Numerous studies have demonstrated the advantages of coordinating connected and autonomous vehicles (CAVs) using control and optimization approaches across various traffic scenarios [1], [2], [3]. In recent years, numerous control approaches have been presented for the coordination of CAVs, assuming a 100% penetration rate. These approaches include time and energy-optimal control strategies [4], [5], [6], [7], [8], [9], model predictive control (MPC) [10], [11], [12], and reinforcement learning (RL) [13], [14], [15] (see [16], [17], [18], [19] for surveys). However, a transportation network with a 100% CAV penetration rate is not expected to be realized by 2060 [20]. As CAVs will gradually and slowly penetrate the market and co-exist with human-driven vehicles (HDVs) in the following decades, addressing planning, control, and navigation for CAVs in mixed traffic, given various human driving styles, is imperative.

Several studies have shown that controlling individual automated vehicles (AVs) may not be sufficient to enhance the overall traffic condition. For example, Wang et al. [21] showed that ego-efficient lane-changing control strategies for AVs (without coordination between vehicles) are beneficial to the entire traffic flow only if the penetration rate of AVs is less than 50%. Thus, AVs should be connected to share information and be coordinated to benefit the entire mixed traffic. However, this problem imposes significant challenges for several reasons. First, control methods for CAVs need to integrate human driving behavior and human–AV interaction to some extent. Approaches not accounting for these factors may result in conservative CAV behavior to prioritize safety, potentially leading to efficiency degradation. Moreover, optimizing the behavior for CAVs requires not only some standard metrics such as safety, fuel economy, or average travel time but also social metrics such as motion naturalness and human comfort [22], which can, at times, be challenging to quantify. Finally, both learning and control methods must be computationally efficient and scalable for real-time implementation. Therefore, in this article, we aim to address the coordination problem for CAVs at merging in mixed-traffic environment.

B. Literature Review

In this section, we summarize the state of the art related to planning, control, and navigation for CAVs in mixed traffic. A significant number of articles have considered connected cruise control or platoon formation for CAVs in mixed traffic [23], [24], [25], [26], [27], [28], where the main objective is to

Manuscript received 31 October 2023; revised 22 April 2024; accepted 28 June 2024. This work was supported by the National Science Foundation (NSF) under Grant CNS-2149520 and Grant CMMI-2219761. Recommended by Associate Editor F. Borrelli. *(Corresponding author: Viet-Anh Le.)*

Viet-Anh Le is with the Department of Mechanical Engineering, University of Delaware, Newark, DE 19716 USA, and also with the Systems Engineering Field, Cornell University, Ithaca, NY 14850 USA (e-mail: vl299@cornell.edu).

Behdad Chalaki was with the Department of Mechanical Engineering, University of Delaware, Newark, DE 19716 USA. He is now with Honda Research Institute USA, Inc., Ann Arbor, MI 48103 USA (e-mail: behdad_chalaki@honda-ri.com).

Filippos N. Tzortzoglou and Andreas A. Malikopoulos are with the School of Civil and Environmental Engineering, Cornell University, Ithaca, NY 14850 USA (e-mail: ft253@cornell.edu; amaliko@cornell.edu).

Digital Object Identifier 10.1109/TCST.2024.3433206

guarantee string stability between CAVs and HDVs. However, in this section, we focus more on research efforts that address the problem in traffic scenarios such as merging at roadways and roundabouts, crossing intersections, and lane-merging or passing maneuvers. In these scenarios, vehicles must complete the tasks not only safely but also efficiently, e.g., improving travel time, avoiding gridlocks, and minimizing traffic disruption and human discomfort. These problems present a more intricate challenge due to their multiobjective nature. The current state-of-the-art methods of planning, control, and navigation for CAVs in "interaction-driven" mixed-traffic scenarios can be roughly classified into two main and emerging categories: *RL* and *optimization-based methods*.

1) RL: In approaches using RL, the aim is to learn control policies for CAVs, usually trained using deep neural networks and trajectories obtained from traffic simulation [29], [30], [31]. To enhance the social coordination of RL policies with human drivers, the concept of social value orientation (SVO) was incorporated into the reward functions [32], [33]. RL algorithms generally do not guarantee real-time safety constraints, so such approaches might need to be combined with other techniques for safety-critical control, such as with control barrier function [34], or lower level MPC [35]. Inverse RL [36] or imitation learning [37] have been used to learn the reward functions of human drivers and demonstrate how CAVs can perform human-like behaviors.

2) Optimization-Based Methods: Such methods include optimal control and MPC to find the control actions for the CAVs. A large number of control methods have been built upon MPC since it can handle multiple objectives and constraints. It exploits the benefits of long-term planning and replanning at every time step to be robust against uncertainty caused by drivers. Some examples of MPC approaches include game-theoretic MPC [38], [39], [40], [41], [42], socially compatible MPC [43], [44], stochastic MPC [45], [46], [47], learning-based MPC [48], [49], [50], and MPC with weight adaptation [51], [52]. In addition, some recent studies used an optimal control framework based on Hamiltonian analysis for improving both time and energy efficiency simultaneously [53], [54], [55].

The aforementioned research efforts have addressed the planning, control, and navigation problems for CAVs at a single-vehicle level. At the same time, only a limited number of research articles have attempted to address the coordination problem in mixed traffic for multiple CAVs using RL [56], [57] and optimization-based methods [58], [59], [60], [61], [62], [63]. Yan and Wu [56] presented a multiagent RL framework for CAVs in a network level while a car-following model simulates the human drivers. Peng et al. [57] considered two CAVs that navigate multiple HDVs to form platoons and cross through a signal-free intersection using deep RL. Addresing the similar problem to [57], Faris et al. [58] utilized mixed-integer optimization for deriving the optimal order of the platoons crossing the intersections. Buckman et al. [59] presented a centralized algorithm for socially compliant navigation at an intersection, given the social preferences of the vehicles. Ghosh and Parisini [60] and Suriyarachchi et al. [61] formulated the mixed-integer optimization problems to coordinate CAVs and traffic lights in mixed traffic. Liu et al. [62] presented a recursive optimal control method utilizing a control barrier function and a control Lyapunov function for coordinating a group of three vehicles where two of them are CAVs at a mixed-traffic on-ramp merging. In [63], we presented a control framework that aims to derive time-optimal trajectories for CAVs in a mixed-traffic merging scenario given the HDVs' future trajectories predicted from Newell's car-following model [64]. The time-optimal trajectories are then combined with a safety filter based on control barrier functions.

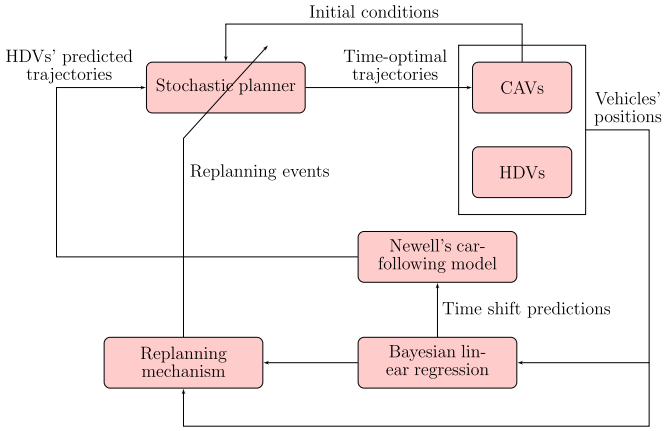

Fig. 1. Diagram illustrating the proposed framework.

C. Our Contributions

In this article, we propose a framework for trajectory planning based on stochastic control that can guarantee *optimal, interaction-aware, robust, and safe* maneuvers for CAVs in mixed-traffic merging scenarios. First, we consider the time-optimal control problem for trajectory planning of the CAVs, which utilizes the closed-form solution of a low-level energy-optimal control problem and satisfies state, input, and safety constraints [4]. Since the trajectory planning problem requires a specific prediction model for HDV's future trajectories, we use a *data-driven Newell's car-following model* in which the time shift, a parameter that characterizes the personal driving behavior, is learned online using *Bayesian linear regression* (BLR). The use of data-driven Newell's car-following model with BLR allows us to not only predict the future trajectory and merging time of each HDV but also quantify the level of uncertainty in the predictions. Using the predictions, we formulate a stochastic time-optimal control problem in which the safety constraints are formulated as probabilistic constraints for robustness without over-conservatism. To address the potential discrepancy between the prediction model and the actual behavior of HDVs, we develop a *replanning mechanism* based on checking the accuracy of the last stored BLR prediction for each HDV with the actual observation. The overall structure of our proposed framework can also be illustrated in Fig. 1. We validate the proposed framework's effectiveness in ensuring safe maneuvers and improving travel time through numerical simulations conducted in commercial software.

In summary, the main contributions of this article are threefold.

1) We use a data-driven Newell's car-following model where BLR is utilized to calibrate the time shift for each human driver.
2) We formulate a stochastic time-optimal control problem with probabilistic constraints to derive robust trajectories for CAVs.
3) We develop a replanning mechanism based on assessing the accuracy of the BLR predictions.

D. Comparison With Related Work

This work differs from the existing work in the literature that considered the problem of multiple CAVs in mixed traffic [56], [57], [58], [59], [60], [61], [62] in the following aspects. First, while the framework in [57] and [58] considered the problem where two CAVs navigate multiple HDVs to form platoons and cross intersections, our framework does not impose such platooning assumptions. Buckman et al. [59], Ghosh and Parisini [60], and Suriyarachchi et al. [61] addressed mixed-traffic scenarios with traffic lights, whereas this work focuses on controlling CAVs in unsignalized merging scenarios. Yan and Wu [56] addressed the mixed-traffic problem at a network level without considering the personal driving behavior of human drivers, while we focus on an isolated traffic scenario where human driving behavior is taken into account. The problem setup in [62] is the most similar to ours, but the presented method focuses on coordinating three vehicles, two of which are CAVs, necessitating high penetration rates of CAVs. In contrast, our framework does not rely on that specific setup of vehicle groups, making it flexible to varying levels of penetration rates.

This article also advances the methods presented in our preliminary work [63], [65] as follows. First, in [65], we employed the stochastic time-optimal control problem to address the coordination problem of 100% CAVs, taking into account uncertainty resulting from low-level tracking or noisy measurements. Meanwhile, this article considered mixed traffic, where uncertainty arises from various human driving behaviors. In [63], we considered mixed-traffic merging scenarios in a deterministic setting in which the trajectories of HDVs are predicted using Newell's car-following model, with parameters approximated by constants averaged from past data. In contrast, this article utilizes BLR to learn the parameters of Newell's car-following model, leading to stochastic trajectory predictions for the HDVs. Finally, we propose a replanning mechanism to account for the inaccuracy of the model, which was not considered in both [63] and [65].

E. Organization

The remainder of this article is organized as follows. In Section II, we formulate the problem of coordinating CAVs in a mixed-traffic merging scenario and provide the preliminary on time-optimal trajectory planning in a deterministic setting. In Section III, we present the data-driven Newell's car-following model with BLR for predicting the future trajectories of HDVs. In Section IV, we develop a stochastic trajectory planning mechanism. Finally, in Section V, we numerically validate the effectiveness of the proposed framework in a simulation environment, and we draw concluding remarks in Section VI.

II. Problem Formulation and Preliminaries

In this section, we first introduce the problem of effectively coordinating multiple CAVs in a merging scenario, considering the presence of HDVs. Subsequently, we provide the preliminary materials on deterministic time-optimal trajectory planning for CAVs based on an earlier optimal control framework [4].

A. Problem Formulation

We consider the problem of coordinating multiple CAVs, co-existing with HDVs, in a merging scenario (Fig. 2), where two merging roadways intersect at a position called a merging point. We define a *control zone* and a *buffer zone*, located upstream of the control zone, which is represented by blue and yellow areas, respectively, in Fig. 2. Within the control zone, the CAVs are controlled by the proposed framework, while in the buffer zone, CAVs are controlled using adaptive cruise control methods. We consider that a *coordinator* is available who has access to the positions of all vehicles (including HDVs and CAVs). The coordinator starts collecting trajectory data of any HDVs once they enter the buffer zone so that at the control zone entry, the data are sufficient for learning the first BLR model (see Section III). We consider that the CAVs and the coordinator can exchange information inside the control zone and buffer zone. Next, we provide some necessary definitions for our exposition.

Definition 1: Let $\mathcal{L}(t) = \{1, \dots, L(t)\}$, $t \in \mathbb{R}_{\geq 0}$, be the set of vehicles traveling inside the control zone, where $L(t) \in \mathbb{N}$ is the total number of vehicles. Let $\mathcal{A}(t) \subset \mathcal{L}(t)$ and $\mathcal{H}(t) \subset \mathcal{L}(t)$ be the sets of CAVs and HDVs, respectively. Note that the indices of the vehicles are determined by the order in which they enter the control zone.

Definition 2: For a vehicle $i \in \mathcal{L}(t)$, let $\mathcal{R}_{i,\mathrm{S}}(t) \subset \mathcal{L}(t)$ and $\mathcal{R}_{i,\mathrm{N}}(t) \subset \mathcal{L}(t)$, $t \in \mathbb{R}_{\geq 0}$, be the sets of vehicles inside the control zone traveling on the same road as vehicle i and on the neighboring road, respectively.

Let p^0, p^{m}, and $p^{\mathrm{f}} \in \mathbb{R}$ be the positions of the control zone entry, the merging point, and the control zone exit, respectively. Without loss of generality, we can set $p^{\mathrm{m}} = 0$. We consider that the dynamics of each vehicle $i \in \mathcal{L}(t)$ are described by a double integrator model as follows:

$$\begin{aligned} \dot{p}_i(t) &= v_i(t) \\ \dot{v}_i(t) &= u_i(t) \end{aligned} \tag{1}$$

where $p_i \in \mathcal{P}$, $v_i \in \mathcal{V}$, and $u_i \in \mathcal{U}$ denote the longitudinal position of the rear bumper, speed, and control input (acceleration/deceleration) of the vehicle, respectively. The sets $\mathcal{P}$, $\mathcal{V}$, and $\mathcal{U}$ are compact subsets of $\mathbb{R}$. The control input is bounded by

$$u_{\min} \leq u_i(t) \leq u_{\max}, \quad \forall i \in \mathcal{L}(t) \tag{2}$$

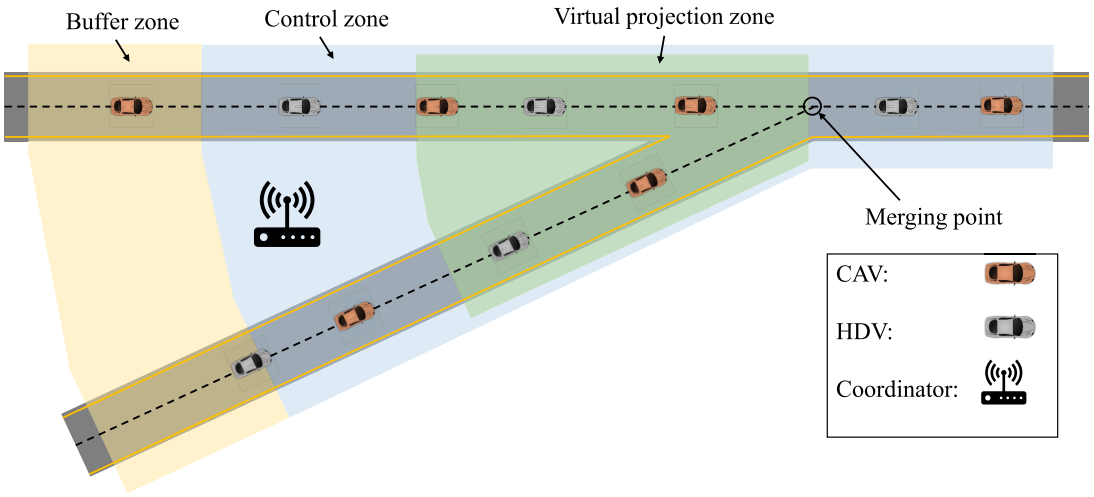

Fig. 2. Merging scenario with two roadways intersecting at a merging point. The control zone and buffer zone are represented by the blue and yellow areas, respectively. In the virtual projection zone (green area), virtual projection is utilized (see Section III).

where $u_{\min} < 0$ and $u_{\max} > 0$ are the minimum and maximum control inputs, respectively, as designated by the physical acceleration and braking limits of the vehicles, or limits that can be imposed for driver/passenger comfort. Next, we consider the speed limits of the CAVs

$$v_{\min} \le v_i(t) \le v_{\max}, \quad \forall i \in \mathcal{L}(t) \tag{3}$$

where $v_{\min} > 0$ and $v_{\max} > 0$ are the minimum and maximum allowable speeds. Note that HDVs can violate the imposed speed limits. However, we make the following assumption.

Assumption 1: The speed of HDVs is always positive, i.e., $v_j(t) > 0, \ \forall j \in \mathcal{H}(t)$.

In practice, if HDVs come to a temporary full stop, Assumption 1 can still be satisfied by assuming a sufficiently small lower bound on the speed.

Next, let t_i^0, t_i^{m}, and $t_i^{\mathrm{f}} \in \mathbb{R}_{\ge 0}$ be the times at which each vehicle i enters the control zone, reaches the merging point, and exits the control zone, respectively. To avoid conflicts between vehicles in the control zone, we impose two constraints: 1) lateral constraints between vehicles traveling on different roads and 2) rear-end constraints between vehicles traveling on the same road. Specifically, to prevent a potential conflict between CAV–i and a vehicle $k \in \mathcal{R}_{i,\mathrm{N}}(t)$ traveling on the neighboring road, we require a minimum time gap $\delta_{\mathrm{l}} \in \mathbb{R}_{\ge 0}$ between the time instants t_i^{m} and t_k^{m} when the CAV–i and vehicle k cross the merging point, i.e.,

$$|t_i^{\mathrm{m}} - t_k^{\mathrm{m}}| \ge \delta_{\mathrm{l}}. \tag{4}$$

To prevent rear-end collision between CAV–i and its immediate preceding vehicle k traveling on the same road, i.e., $k = \max\{j \in \mathcal{R}_{i,\mathrm{S}}(t) \mid j < i\}$, we impose the following rear-end safety constraint:

$$p_k(t - \delta_{\mathrm{r}}) - p_i(t) \ge d_{\min}, \ t \in \left[t_i^0, t_k^{\mathrm{f}}\right] \tag{5}$$

where $d_{\min} \in \mathbb{R}_{\ge 0}$ and $\delta_{\mathrm{r}} \in \mathbb{R}_{\ge 0}$ are the minimum distance at a standstill and safe time gap. Note that $p_k(t - \delta_{\mathrm{r}})$ denotes the position of vehicle k at time instant $t - \delta_{\mathrm{r}}$. In addition, we need to guarantee the rear-end safety constraint (5) after the merging point between each CAV–i and a vehicle $k \in \mathcal{R}_{i,\mathrm{N}}(t)$ entering the control zone on the neighboring road and crosses the merging point immediately before CAV–i as follows:

$$p_k(t - \delta_{\mathrm{r}}) - p_i(t) \ge d_{\min}, \ t \in \left[t_i^{\mathrm{m}}, t_k^{\mathrm{f}}\right] \tag{6}$$

for $k = \max\{j \in \mathcal{R}_{i,\mathrm{N}}(t) \mid t_j^{\mathrm{m}} < t_i^{\mathrm{m}}\}$.

B. Time-Optimal Trajectory Planning

Next, we explain the deterministic time-optimal trajectory planning framework developed initially for coordinating CAVs with a 100% penetration [4]. We start the exposition with the unconstrained solution of an energy-optimal control problem for each CAV–i [5]. Given a fixed t_i^{f} that CAV–i exits the control zone, the energy-optimal control problem aims at finding the optimal control input (acceleration/deceleration) for each CAV by solving the following problem.

Problem 1 (Energy-Optimal Control Problem): Let t_i^0 and t_i^{f} be the times that CAV–i enters and exits the control zone, respectively. The energy-optimal control problem for CAV–i at t_i^0 is given by

$$\begin{aligned}
&\underset{u_i(t)\in\mathcal{U}}{\text{minimize}} \quad \frac{1}{2}\int_{t_i^0}^{t_i^{\mathrm{f}}} u_i^2(t)\ \mathrm{d}t,\\
&\text{subject to:}\\
&\quad (1),\ (2),\ (3),\\
&\quad (5),\ k = \max\left\{j \in \mathcal{R}_{i,\mathrm{S}}\left(t_i^0\right) \mid j < i\right\},\\
&\quad (6),\ k = \max\left\{j \in \mathcal{R}_{i,\mathrm{N}}\left(t_i^0\right) \mid t_j^{\mathrm{m}} < t_i^{\mathrm{m}}\right\},\\
&\text{given:}\\
&\quad p_i\left(t_i^0\right) = p^0,\ v_i\left(t_i^0\right) = v_i^0,\ p_i\left(t_i^{\mathrm{f}}\right) = p^{\mathrm{f}}
\end{aligned} \tag{7}$$

where v_i^0 is the speed of CAV–i at the entry point. The boundary conditions in (7) are set at the entry and exit of the control zone.

The closed-form solution of Problem 1 for each CAV–i can be derived using the Hamiltonian analysis [66]. If none of the state and control constraints are active, the closed-form optimal control law and trajectory are given by [4]

$$u_i(t) = 6\phi_{i,3}t + 2\phi_{i,2}$$

$$v_i(t) = 3\phi_{i,3}t^2 + 2\phi_{i,2}t + \phi_{i,1}$$
$$p_i(t) = \phi_{i,3}t^3 + \phi_{i,2}t^2 + \phi_{i,1}t + \phi_{i,0} \tag{8}$$

where $\phi_{i,3}, \phi_{i,2}, \phi_{i,1}, \phi_{i,0} \in \mathbb{R}$ are the constants of integration. Since the speed of CAV–i is not specified at the exit time t_i^{f}, we consider the boundary condition

$$u_i\left(t_i^{\mathrm{f}}\right) = 0. \tag{9}$$

For the full derivation of the closed-form solution in (8) using Hamiltonian analysis, the readers are referred to [4].

Given the boundary conditions in (7) and (9), and considering t_i^{f} is known, the constants of integration can be found by

$$\boldsymbol{\phi}_i = \begin{bmatrix} \phi_{i,3} \\ \phi_{i,2} \\ \phi_{i,1} \\ \phi_{i,0} \end{bmatrix} = \begin{bmatrix} \left(t_i^0\right)^3 & \left(t_i^0\right)^2 & t_i^0 & 1 \\ 3\left(t_i^0\right)^2 & 2t_i^0 & 1 & 0 \\ \left(t_i^{\mathrm{f}}\right)^3 & \left(t_i^{\mathrm{f}}\right)^2 & t_i^{\mathrm{f}} & 1 \\ 6t_i^{\mathrm{f}} & 2 & 0 & 0 \end{bmatrix}^{-1} \begin{bmatrix} p^0 \\ v_i^0 \\ p^{\mathrm{f}} \\ 0 \end{bmatrix}. \tag{10}$$

Note that using the Cardano et al.'s [67] method, the time trajectory $t_i(p_i)$ as a function of the position is given by

$$t_i(p_i) = \sqrt[3]{-\frac{1}{2}\left(\omega_{i,1} + \omega_{i,2}\ p_i\right) + \sqrt{\frac{1}{4}\left(\omega_{i,1} + \omega_{i,2}\ p_i\right)^2 + \frac{1}{27}\omega_{i,0}^3}} + \sqrt[3]{-\frac{1}{2}\left(\omega_{i,1} + \omega_{i,2}\ p_i\right) - \sqrt{\frac{1}{4}\left(\omega_{i,1} + \omega_{i,2}\ p_i\right)^2 + \frac{1}{27}\omega_{i,0}^3}} + \omega_{i,3}, \qquad p_i \in \mathcal{P} \tag{11}$$

$$\omega_{i,0} = \frac{\phi_{i,1}}{\phi_{i,3}} - \frac{1}{3}\left(\frac{\phi_{i,2}}{\phi_{i,3}}\right)^2 \tag{12}$$

$$\omega_{i,1} = \frac{1}{27}\left[2\left(\frac{\phi_{i,2}}{\phi_{i,3}}\right)^3 - \frac{9\phi_{i,2}\cdot\phi_{i,1}}{(\phi_{i,3})^2}\right] + \frac{\phi_{i,0}}{\phi_{i,3}} \tag{13}$$

$$\omega_{i,2} = -\frac{1}{\phi_{i,3}}, \qquad \omega_{i,3} = -\frac{\phi_{i,2}}{3\phi_{i,3}} \tag{14}$$

where $\omega_{i,3}, \omega_{i,2}, \omega_{i,1}$, and $\omega_{i,0} \in \mathbb{R}$ such that $(1/4)(\omega_{i,1} + \omega_{i,2}\ p_i)^2 + (1/27)\omega_{i,0}^3 > 0$, and they are all defined in terms of $\phi_{i,3}, \phi_{i,2}, \phi_{i,1}, \phi_{i,0} \in \mathbb{R}$, with $\phi_{i,3} \neq 0$. The algebraic derivation of (11) is standard [4] and thus omitted. We use (11) to compute the merging time t_i^{m}.

Next, we formulate the time-optimal control problem to minimize the travel time and guarantee all the constraints for CAVs given the energy-optimal trajectory (8) at t_i^0. We enforce this unconstrained trajectory as a motion primitive to avoid the complexity of solving a constrained optimal control problem by piecing constrained and unconstrained arcs together [5]. We refer to this problem as *deterministic planning problem* to differentiate it from the stochastic problems discussed in Section IV.

Problem 2 (Deterministic Planning at the Control Zone Entry): At the time t_i^0 of entering the control zone, let $\mathcal{T}_i(t_i^0) = [\underline{t}_i^{\mathrm{f}}, \overline{t}_i^{\mathrm{f}}]$ be the feasible range of travel time under the state and input constraints of CAV–i computed at t_i^0. The formulation for computing $\underline{t}_i^{\mathrm{f}}$ and $\overline{t}_i^{\mathrm{f}}$ can be found in [68]. Then, CAV–i solves the following time-optimal control problem to find the minimum exit time $t_i^{\mathrm{f}} \in \mathcal{T}_i(t_i^0)$ that satisfies all state, input, and safety constraints:

$$\begin{aligned} &\underset{t_i^{\mathrm{f}} \in \mathcal{T}_i(t_i^0)}{\text{minimize}} \quad t_i^{\mathrm{f}} \\ &\text{subject to:} \\ &\quad (2), (3), \\ &\quad (4),\ \forall k \in \mathcal{R}_{i,\mathrm{N}}\left(t_i^0\right), \\ &\quad (5),\ k = \max\left\{j \in \mathcal{R}_{i,\mathrm{S}}\left(t_i^0\right) \mid j < i\right\}, \\ &\quad (6),\ k = \max\left\{j \in \mathcal{R}_{i,\mathrm{N}}\left(t_i^0\right) \mid t_j^{\mathrm{m}} < t_i^{\mathrm{m}}\right\}, \\ &\quad (8), \\ &\text{given:} \\ &\quad p_i\left(t_i^0\right) = p^0,\ v_i\left(t_i^0\right) = v_i^0, \\ &\quad p_i\left(t_i^{\mathrm{f}}\right) = p^{\mathrm{f}},\ u_i\left(t_i^{\mathrm{f}}\right) = 0. \end{aligned} \tag{15}$$

The computation steps for numerically solving Problem 2 are summarized as follows or can also be found in [68]. First, we initialize $t_i^{\mathrm{f}} = \underline{t}_i^{\mathrm{f}}$ and compute the parameters $\boldsymbol{\phi}_i$ using (10). We evaluate all the state, control, and safety constraints. If none of the constraints is violated, we return the solution; otherwise, t_i^{f} is increased by a step size. The procedure is repeated until the solution satisfies all the constraints. By solving Problem 2, the optimal exit time t_i^{f} along with the optimal trajectory and control law (8) are obtained for CAV–i for $t \in [t_i^0, t_i^{\mathrm{f}}]$.

Remark 1: If a feasible solution to Problem 2 exists, then the solution is a cubic polynomial that guarantees none of the constraints become active. In case the solution of Problem 2 does not exist, we can derive the optimal trajectory for the CAVs by piecing together the constrained and unconstrained arcs until the solution does not violate any constraints (see [5]).

III. Human Drivers' Trajectory Prediction

To solve the trajectory planning problem for CAV–i, the trajectories and merging times of all vehicles having potential conflicts with CAV–i must be available. When CAV–i enters the control zone, the time trajectories of all CAVs traveling inside the control zone can be obtained from the coordinator. However, the time trajectories of the HDVs are not known. Next, we propose an approach to predict the trajectories of the HDVs traveling inside the control zone by combining Newell's car-following model [64] and BLR [69, Chapter 3].

A. Bayesian Linear Regression

Consider $N \in \mathbb{R}$ noisy observations y_i of a linear model with Gaussian noise: $y_i = \boldsymbol{\theta}^\top \boldsymbol{x}_i + e_i$, for $i = 1, \ldots, N$, where $\boldsymbol{\theta} \in \mathbb{R}^M$, $M \in \mathbb{N}$ is the vector of weights, $\boldsymbol{x}_i \in \mathbb{R}^M$ is the vectors of inputs, and $e_i \sim \mathcal{N}(0, \beta^{-1})$ is the Gaussian noise where $\beta \in \mathbb{R}_{\geq 0}$ is the precision (the inverse of variance). Let $\mathcal{O} = (\boldsymbol{X}, \boldsymbol{Y})$ be the tuple of observation data for inputs and outputs, where $\boldsymbol{X} = [\boldsymbol{x}_1^\top, \ldots, \boldsymbol{x}_N^\top]^\top \in \mathbb{R}^{M\times N}$ and $\boldsymbol{Y} = [y_1, \ldots, y_N]^\top \in \mathbb{R}^N$. The goal of BLR is to find the maximum likelihood estimate for $\boldsymbol{\theta}$ given the observation data.

The maximum a posteriori (MAP) estimate of $\boldsymbol{\theta}$ can be found by maximizing the log of the posterior distribution [69, Chapter 3]. If we assume a Gaussian prior over the

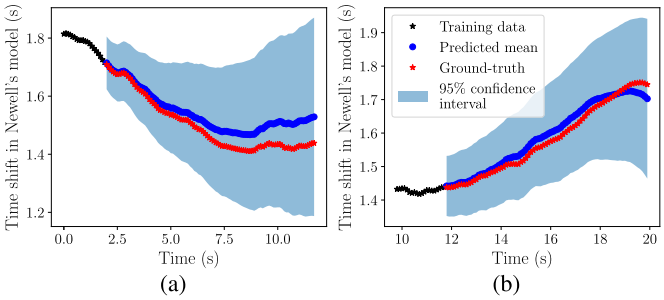

Fig. 3. Time-shift prediction from BLR used to calibrate Newell's car-following model for a HDV in Lyft level-5 open dataset [70]. (a) First model is trained using the initial 20 data points and (b) second model is trained with more recent data if the first model yields high predicted variances.

weights $\boldsymbol{\theta} \sim \mathcal{N}(\mathbf{0}, \alpha^{-1}\boldsymbol{I}_M)$ where $\alpha \in \mathbb{R}_{\geq 0}$ is the precision and $\boldsymbol{I}_M$ is the $M \times M$ identity matrix, and the Gaussian likelihood $\mathbb{P}(\boldsymbol{Y} \mid \boldsymbol{X}, \boldsymbol{\theta}, \beta) = \mathcal{N}(\boldsymbol{\theta}^\top \boldsymbol{X}, \beta^{-1}\boldsymbol{I}_N)$, then the log of the posterior distribution is computed as follows:

$$\log \mathbb{P}(\boldsymbol{\theta} \mid \boldsymbol{Y}, \boldsymbol{X}, \alpha, \beta) = -\beta \mathcal{E}(\boldsymbol{\theta}) - \frac{1}{2}\alpha \boldsymbol{\theta}^\top \boldsymbol{\theta} + c \tag{16}$$

where c is a constant and $\mathcal{E}(\boldsymbol{\theta})$ is the sum-of-squares error function coming from the exponent of the likelihood function, which is computed by

$$\mathcal{E}(\boldsymbol{\theta}) = \frac{1}{2}\sum_{i=1}^{N}\left(y_i - \boldsymbol{\theta}^\top \boldsymbol{x}_i\right)^2 = \frac{1}{2}\|\boldsymbol{Y} - \boldsymbol{X}\boldsymbol{\theta}\|_2^2. \tag{17}$$

Thus, the MAP estimate of $\boldsymbol{\theta}$ has the following analytical solution:

$$\boldsymbol{\mu}_{\boldsymbol{\theta}} = \beta \boldsymbol{\Sigma}_{\boldsymbol{\theta}} \boldsymbol{X}^\top \boldsymbol{Y} \tag{18}$$

$$\boldsymbol{\Sigma}_{\boldsymbol{\theta}}^{-1} = \beta \boldsymbol{X}^\top \boldsymbol{X} + \alpha \boldsymbol{I}_m \tag{19}$$

while estimates for priors, i.e., α and β, can be obtained by the empirical Bayes method (also known as maximum marginal likelihood [69]).

Once the BLR model is trained, the posterior predictive distribution for $\boldsymbol{\theta}$ is a Gaussian distribution $\mathcal{N}(\boldsymbol{\mu}_{\boldsymbol{\theta}}, \boldsymbol{\Sigma}_{\boldsymbol{\theta}})$ with the mean and covariance matrix given in (18). At a new input $\boldsymbol{x}_*$, the predicted mean and variance are given by

$$\mu_* = \boldsymbol{\mu}_{\boldsymbol{\theta}}^\top \boldsymbol{x}_* \tag{20}$$

$$\sigma_*^2 = \boldsymbol{x}_*^\top \boldsymbol{\Sigma}_{\boldsymbol{\theta}} \boldsymbol{x}_* + \beta^{-1}. \tag{21}$$

BLR is highly suitable for online learning implementation due to its light computation, where the complexity generally is $\mathcal{O}(M^2 N)$, i.e., it scales linearly with the training data size and quadratically with the input dimension. Moreover, we can check for retraining by comparing the new observation to the confidence interval or by considering prediction uncertainty. This approach can avoid overly frequent model retraining.

B. Data-Driven Newell's Car-Following Model With BLR

Newell's car-following model [64] considers that the position of each vehicle is shifted in time and space from its preceding vehicle's trajectory due to the effect of traffic wave propagation. Specifically, the position of each HDV–k, $k \in \mathcal{H}(t)$, is predicted from the position of its preceding vehicle j as follows:

$$p_k(t) = p_j(t - \tau_k) - w\,\tau_k \tag{22}$$

where $\tau_k \in \mathbb{R}_{\geq 0}$ is the time shift of HDV–k, and $w \in \mathbb{R}_{\geq 0}$ is the speed of the backward propagating congestion waves, which is considered to be a constant [71], [72]. The time shift τ_k is considered a stochastic variable and can be learned by BLR. Since $v_j(t) > 0$ (Assumption 1) and $w > 0$, $p_j(t - \tau_k) - w\tau_k$ is a strictly decreasing function of τ_k. Thus, there exists a unique value of τ_k such that (22) is satisfied for any t. In this article, rather than only using the data at a specific time instant, we use the observations over a finite estimation horizon of length $H \in \mathbb{Z}^+$ to estimate the distribution of τ_k for each HDV–k by a BLR model as follows:

$$\tau_k \sim \mathcal{B}_k(\boldsymbol{x}_k; \boldsymbol{\theta}_k) \tag{23}$$

where $\mathcal{B}_k$ denotes the BLR model, $\boldsymbol{x}_k = [1, p_k, p_j]^\top \in \mathbb{R}^3$ is the vector of inputs, and $\boldsymbol{\theta}_k \in \mathbb{R}^3$ is the vector of weights. Henceforth, for ease of notation, we use $\mathcal{B}_k(p_k, p_j)$ to denote the BLR model for τ_k given a preceding vehicle j.

To demonstrate the model's capability to accurately learn realistic human driving behavior, we utilized the trajectory data for a specific human driver in Lyft level-5 open dataset [70] whose actual time shift varies between 1.4 and 1.8 s. The predicted time shift with 95% confidence interval using BLR is shown in Fig. 3. We utilized $N = 20$ initial data points to train a BLR model [Fig. 3(a)] and retrain the model [Fig. 3(b)] with more recent data if either the BLR prediction uncertainty is too high or the actual observations are outside the 95% confidence interval.

Note that in the merging scenario, we consider the virtual projection of vehicles traveling on that road to capture the lateral interaction of each HDV with vehicles on the neighboring road. The virtual projection is implemented in a proximity area before the merging point, defined as the virtual projection zone in Fig. 2. The virtual projection is illustrated by an example in Fig. 4. We consider that from the perspective of HDV–3, the projected CAV–2 is the preceding vehicle instead of CAV–1. Similar generalized car-following models for capturing the merging behavior of human drivers have been presented in [73], [74], and [75].

C. Exception Handling

Next, we present a method to handle the case when an HDV, e.g., HDV–k, is not preceded by any vehicles in the control zone, including those determined by virtual projection. Generally, it is reasonable to assume that HDV–k remains its current speed in this case. However, to further quantify the uncertainty in human driving behavior by exploiting the data-driven Newell's car-following model, we consider that HDV–k follows *a virtual preceding vehicle* with a constant speed trajectory. Let k' denote the virtual preceding vehicle to HDV–k. The constant speed trajectory of the virtual preceding vehicle is given by

$$p_{k'}(t) = \phi_{k',1}\, t + \phi_{k',0} \tag{24}$$

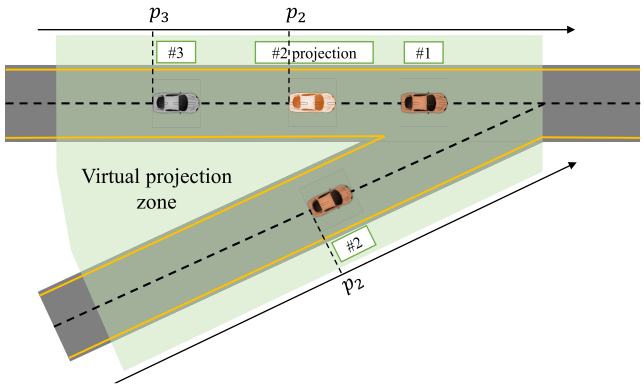

Fig. 4. Example of virtual projection in the virtual projection zone, where the CAV–2 is projected from the perspective of HDV–3.

$$v_{k'}(t) = \phi_{k',1} \tag{25}$$

where $\phi_{k',1} \in \mathbb{R}_{\geq 0}$ and $\phi_{k',0} \in \mathbb{R}$ are the constants, in which $\bar{\phi}_{k',1}$ is computed based on the average speed of HDV–k over the estimation horizon, while $\phi_{k',0}$ is chosen such that $p_{k'}(t_k^0 - \bar{\tau}) = p^0$ with $\bar{\tau} \in \mathbb{R}_{\geq 0}$ is an arbitrarily predefined constant. We consider that the actual position trajectory of HDV–k is computed by Newell's car-following model given the virtual preceding vehicle k' as follows:

$$p_k(t) = p_{k'}(t - \tau_k) - w\tau_k = \phi_{k',1}\,(t - \tau_k) + \phi_{k',0} - w\tau_k \tag{26}$$

where we quantify τ_k with a BLR model $\tau_k \sim \mathcal{B}(p_k, p_{k'})$, which is similar to (23).

IV. Stochastic Planning With Probabilistic Constraints

In this section, we develop a stochastic trajectory planning framework using the data-driven Newell's car following model for learning human driving behavior presented in Section III. The use of stochastic control can reduce the conservatism of classical robust control for uncertain systems by formulating robust constraints as probabilistic constraints [76]. As a result, probabilistic constraints have been used recently in robust trajectory optimization algorithms [77], [78], [79].

A. Uncertainty Quantification

Remark 2: In our framework, we consider that the trajectories of CAVs are deterministic, or equivalently, stochastic variables with zero variances.

Note that given the data-driven Newell's car-following model using BLR, the time shift τ_k of HDV–k at any future time t must satisfy the following equation:

$$\tau_k(t) \sim \mathcal{B}\big(p_j(t - \tau_k(t)) - w\tau_k(t),\ p_j(t)\big) \tag{27}$$

where j is the index of the preceding vehicle. Solving (27) to obtain a closed-form solution for $\tau_k(t)$ and $p_k(t)$ at any future time t is computationally intractable. As a result, in what follows, we propose a method to simplify the predictions of trajectory and merging time for each HDV–k along with quantifying the uncertainty of the predictions.

When HDV–k enters the control zone at t_k^0, we train the first BLR model $\mathcal{B}_k$ for τ_k using a dataset of $H \in \mathbb{N}$ data points collected in the buffer zone. Let $\tau_k(t_k^0) \sim \mathcal{N}(\mu_{\tau_k}, \sigma_{\tau_k}^2)$ be the prediction of τ_k with the mean μ_{τ_k} and the variance $\sigma_{\tau_k}^2$. We utilize $\tau_k(t_k^0)$ to construct a nominal predicted trajectory and merging time for HDV–k. In our analysis, we consider the *zero-variance method* for approximating uncertainty propagation while making BLR prediction, which implies that if the inputs of a BLR model include a stochastic variable, we only use its mean to compute the mean and variance of the model output without taking its variance into account. The zero-variance method has been considered in multiple studies on using stochastic processes in control [80], [81].

Assumption 2: The effect of uncertainty propagation is approximated by the zero-variance method.

Assumption 2 implies that the trajectory prediction of any HDV only depends on the uncertainty resulting from the time-shift prediction of Newell's car-following model and does not depend on the uncertainty in trajectory prediction of its preceding vehicles. The reason for ignoring full uncertainty propagation is that it may lead to overly conservative constraints if the CAV penetration rate is low. Moreover, Assumption 2 aims to simplify the computation since the distribution of vehicles' trajectories, which are inputs of the BLR model, is generally not Gaussian as we show later (see Lemma 1).

Next, we show that the predicted position mean for any HDVs using the data-driven Newell's car-following model is either a cubic polynomial or an affine polynomial.

Lemma 1: Given Assumption 2, at any time t, if the distribution $\mathcal{N}(\mu_{\tau_k}(t), \sigma_{\tau_k}^2(t))$ for $\tau_k(t)$ is known, and HDV–k is preceded by a vehicle j whose predicted position mean is a cubic polynomial of time parameterized by $\boldsymbol{\phi}_j = [\phi_{j,3}, \phi_{j,2}, \phi_{j,1}, \phi_{j,0}]^\top$, then the predicted position mean and variance of HDV–k at time t can be computed as given by (28) and (29), shown at the bottom of the next page, where $\lambda_k = t - \mu_{\tau_k}$.

Moreover, the coefficients of the polynomial are computed as follows:

$$\begin{aligned}
\phi_{k,3} &= \phi_{j,3} \\
\phi_{k,2} &= \phi_{j,2} - 3\,\phi_{j,3}\,\mu_{\tau_k} \\
\phi_{k,1} &= \phi_{j,1} - 2\,\phi_{j,2}\,\mu_{\tau_k} + 3\,\phi_{j,3}\,\big(\mu_{\tau_k}^2 + \sigma_{\tau_k}^2\big) \\
\phi_{k,0} &= \phi_{j,0} - \big(\phi_{j,1} + w\big)\mu_{\tau_k} + \phi_{j,2}\big(\mu_{\tau_k}^2 + \sigma_{\tau_k}^2\big) \\
&\quad - \phi_{j,3}\mu_{\tau_k}\big(\mu_{\tau_k}^2 + 3\sigma_{\tau_k}^2\big).
\end{aligned} \tag{30}$$

Proof: The proof is given in the Appendix. Note that the distribution of $p_k(t)$ in this case is not Gaussian. □

Lemma 2: Given Assumption 2, if the distribution $\mathcal{N}(\mu_{\tau_k}, \sigma_{\tau_k}^2)$ for $\tau_k(t)$ at time t is known, and HDV–k is preceded by a vehicle j whose predicted position mean is an affine polynomial of time parameterized by $\boldsymbol{\phi}_j = [\phi_{j,1}, \phi_{j,0}]^\top$, i.e., it cruises with constant speed, then the predicted position mean and variance of HDV–k at time t can be computed as follows:

$$\mu_{p_k}(t) = \big(\phi_{j,1} + w\big)\,\lambda_k + \big(\phi_{j,0} - w\,t\big) \tag{31}$$

$$\sigma_{p_k}^2(t) = \big(\phi_{j,1} + w\big)^2 \sigma_{\tau_k}^2 \tag{32}$$

where $\lambda_k = t - \mu_{\tau_k}$ and the coefficients of the polynomial are computed as follows:

$$\begin{aligned}\phi_{k,1} &= \phi_{j,1}\\ \phi_{k,0} &= \phi_{j,0} - \big(\phi_{j,1} + w\big)\mu_{\tau_k}.\end{aligned} \tag{33}$$

Proof: This is a trivial case of Lemma 1 with $\phi_{j,3} = \phi_{j,2} = 0$. □

Theorem 1: The mean prediction for the position of any HDV–k is either a cubic polynomial or an affine polynomial of time.

Proof: Given Lemmas 1 and 2, if HDV–k is preceded by an HDV, e.g., HDV–j, and the mean prediction for the position of HDV–j is either a cubic polynomial or an affine polynomial of time, then that of HDV–k is also either a cubic polynomial or an affine polynomial of time. Therefore, we only need to consider the cases where: 1) HDV–k is preceded by a CAV, e.g., CAV–i or 2) HDV–k is not preceded by any vehicle inside the control zone.

1) *Case 1:* If HDV–k is preceded by CAV–i, since the position trajectory of CAV–i is a cubic polynomial, from Lemma 1, we can verify that the predicted position mean of HDV–k is a cubic polynomial of time.
2) *Case 2:* If HDV–k is not preceded by any vehicle inside the control zone and has not crossed the merging point, from (26), the predicted mean of $p_k(t)$ is

$$\mu_{p_k}(t) = \bar{\phi}_{j,1}\, t + \big(\phi_{j,0} - \bar{\phi}_{j,1}\, \mu_{\tau_k} - w\, \mu_{\tau_k}\big) \tag{34}$$

which is a linear function of time. □

Lemma 3: Suppose HDV–k has not crossed the merging point. Then, the merging time of HDV–k is computed by

$$t_k^{\mathrm{m}} = t_j(w\tau_k) + \tau_k \tag{35}$$

where $t_j(w\tau_k)$ denotes the time that the preceding vehicle j reaches the position $w\tau_k$, where $\tau_k = \tau_k(t_k^0) \sim \mathcal{N}(\mu_{\tau_k}, \sigma_{\tau_k}^2)$.

Proof: Evaluating Newell's car-following model (22) at t_k^{m}, we have

$$p_k\big(t_k^{\mathrm{m}}\big) = p_j\big(t_k^{\mathrm{m}} - \tau_k\big) - w\tau_k. \tag{36}$$

At the merging time, we have $p_k(t_k^{\mathrm{m}}) = p^{\mathrm{m}} = 0$ which results in

$$p_j\big(t_k^{m} - \tau_k\big) = w\tau_k. \tag{37}$$

As the speed of vehicle k is always positive given (3) and Assumption 1, we can compute the inverse as

$$t_k^{m} - \tau_k = t_j(w\tau_k) \tag{38}$$

and the proof is complete. □

If vehicle j is an HDV, we approximate $t_j(w\tau_k)$ by solving $\mu_{p_j} = w\tau_k$. If $\mu_{p_j}(t)$ is an affine polynomial of time parameterized by $\boldsymbol{\phi}_j = [\phi_{j,1}, \phi_{j,0}]^\top$, the time trajectory as a function of position is given by

$$t_j\big(p_j\big) = \frac{-\phi_{j,0}}{\phi_{j,1}}\, p_j \tag{39}$$

while if $\mu_{p_j}(t)$ is a cubic polynomial, the time trajectory follows Cardano formulation (11). Given Lemma 3, t_k^{m} is a stochastic variable with Gaussian distribution, $t_k^{\mathrm{m}} \sim \mathcal{N}(\mu_{t_k^{\mathrm{m}}}, \sigma_{t_k^{\mathrm{m}}}^2)$ with $\mu_{t_k^{\mathrm{m}}} = \mu_{\tau_k} + t_j(w\tau_k)$ and $\sigma_{t_k^{\mathrm{m}}}^2 = \sigma_{\tau_k}^2$. To guarantee that the computation of $t_j(w\tau_k)$ using the polynomial trajectories is valid, the position $w\tau_k$ must be inside the control zone. Thus, we impose the following assumption.

Assumption 3: The speed of the backward propagating congestion waves w is chosen such that $w\,\tau_k \le p^{\mathrm{f}}$.

Assumption 3 can be satisfied in practice since the term $w\,\tau_k$ describes the standstill spacing between vehicles and should be relatively small compared to the length from the merging point to the control zone exit.

B. Stochastic Time-Optimal Control Problem With Probabilistic Constraints

Since the predicted trajectory and merging time for any HDV–k are stochastic variables, next, we formulate probabilistic constraints for rear-end and lateral safety that guarantee constraint satisfaction at a certain probability. Let $\xi \in (0, 1)$ be the probability of constraint satisfaction. The lateral probabilistic constraint for CAV–i and HDV–k entering from different roads is given by

$$\begin{aligned}&\mathbb{P}\big[t_i^{\mathrm{f}} - t_k^{\mathrm{f}} \ge \delta_l\big] \ge \xi\\ \text{OR}\quad &\mathbb{P}\big[t_i^{\mathrm{f}} - t_k^{\mathrm{f}} \le -\delta_l\big] \ge \xi.\end{aligned} \tag{40}$$

The deterministic rear-end constraints for CAV–i and its immediate preceding HDV–k in (5) and (6) are considered as the following probabilistic constraints:

$$\mathbb{P}\big[p_i(t) - p_k(t - \delta_r) \le -d_{\min}\big] \ge \xi,\ \forall t \in \big[t_i^0, t_k^{\mathrm{f}}\big] \tag{41}$$

for $k = \max\{j \in \mathcal{R}_{i,\mathrm{S}}(t) \mid j < i\}$, and

$$\mathbb{P}\big[p_i(t) - p_k(t - \delta_r) \le -d_{\min}\big] \ge \xi,\ \forall t \in \big[t_i^{\mathrm{m}}, t_k^{\mathrm{f}}\big] \tag{42}$$

for $k = \max\{j \in \mathcal{L}(t) \mid t_j^{\mathrm{m}} < t_i^{\mathrm{m}}\}$.

Therefore, we formulate the following stochastic time-optimal control problem for planning at the control zone entry.

Problem 3 (Stochastic Planning at the Control Zone Entry): At the time t_i^0 of entering the control zone, CAV–i solves the following time-optimal control problem:

$$\underset{t_i^{\mathrm{f}} \in \mathcal{T}_i(t_i^0)}{\text{minimize}} \quad t_i^{\mathrm{f}}$$

$$\mu_{p_k}(t) = \phi_{j,3}(\lambda_k^3 + 3\lambda_k\sigma_{\tau_k}^2) + \phi_{j,2}(\lambda_k^2 + \sigma_{\tau_k}^2) + (\phi_{j,1} + w)\lambda_k + (\phi_{j,0} - wt) \tag{28}$$

$$\begin{aligned}\sigma_{p_k}^2(t) = \sigma_{\tau_k}^2\Big(&(\phi_{j,1} + w)^2 + 4(\phi_{j,1} + w)\phi_{j,2}\lambda_k + 6(\phi_{j,1} + w)\phi_{j,3}\lambda_k^2 + 6(\phi_{j,1} + w)\phi_{j,3}\sigma_{\tau_k}^2 + 4\phi_{j,2}^2\lambda_k^2 + 2\phi_{j,2}^2\sigma_{\tau_k}^2\\ &+ 12\phi_{j,2}\phi_{j,3}\lambda_k^3 + 24\phi_{j,2}\phi_{j,3}\lambda_k\sigma_{\tau_k}^2 + 36\phi_{j,3}^2\lambda_k^2\sigma_{\tau_k}^2 + 15\phi_{j,3}^2\sigma_{\tau_k}^4 + 9\phi_{j,3}^2\lambda_k^4\Big).\end{aligned} \tag{29}$$

subject to:

$$\begin{aligned}&(2),\ (3),\ (8),\\ &(40),\ \forall k \in \mathcal{R}_{i,\mathrm{N}}\left(t_i^0\right),\\ &(41),\ k=\max\left\{j \in \mathcal{R}_{i,\mathrm{S}}\left(t_i^0\right) \mid j<i\right\},\\ &(42),\ k=\max\left\{j \in \mathcal{R}_{i,\mathrm{N}}\left(t_i^0\right) \mid t_j^{\mathrm{m}}<t_i^{\mathrm{m}}\right\},\end{aligned}$$

given:

$$\begin{aligned}&p_i\left(t_i^0\right)=p^0,\ v_i\left(t_i^0\right)=v_i^0,\\ &p_i\left(t_i^{\mathrm{f}}\right)=p^{\mathrm{f}},\ u_i\left(t_i^{\mathrm{f}}\right)=0.\end{aligned} \tag{43}$$

Given the uncertainty quantification of stochastic variables we derived in Section IV-A and the constraint tightening technique [79], the lateral probabilistic constraint (40) is equivalent to the following deterministic form:

$$\begin{aligned}&t_i^{\mathrm{f}}-\mu_{t_k^{\mathrm{f}}} \geq \delta_l+z\sigma_{t_k^{\mathrm{f}}}\\ \text{OR}\quad &t_i^{\mathrm{f}}-\mu_{t_k^{\mathrm{f}}} \leq -\delta_l-z\sigma_{t_k^{\mathrm{f}}}\end{aligned} \tag{44}$$

where $z=(2)^{1/2}\,\mathrm{erf}^{-1}(2\xi-1)$ with $\mathrm{erf}^{-1}(\cdot)$ is the inverse error function. Likewise, the rear-end probabilistic constraints (41) and (42) can be, respectively, transformed to deterministic constraints as follows:

$$p_i(t)-\mu_{p_k}(t-\delta_r) \leq -d_{\min}-z\sigma_{p_k}(t-\delta_r),\ \forall t \in \left[t_i^0, t_k^{\mathrm{f}}\right] \tag{45}$$

and

$$p_i(t)-\mu_{p_k}(t-\delta_r) \leq -d_{\min}-z\sigma_{p_k}(t-\delta_r),\ \forall t \in \left[t_i^{\mathrm{m}}, t_k^{\mathrm{f}}\right]. \tag{46}$$

Thus, for solving Problem 3, the probabilistic constraints in (43) are replaced by (44)–(46), which result in an equivalent deterministic optimization problem.

C. Replanning

Since the future trajectory and merging time for any HDV derived in Section IV-A are computed based on the prediction of τ_k at t_k^0, the predictions are not reliable if $\hat{\tau}_k(t)$ at $t > t_k^0$, where $\hat{\tau}_k$ denotes the actual observation of τ_k obtained by solving (22), is highly different to $\tau_k(t_k^0)$. Under this discrepancy, the planned trajectories for the CAVs may not always ensure safe maneuvers. Next, to address this issue, we present a mechanism for replanning based on checking the accuracy of the BLR predictions. First, we define *replanning instances* and how to determine replanning instances as follows.

Definition 3: A time instance $t^{\mathrm{c}} \in \mathbb{R}_{\geq 0}$ is a replanning instance if at t^{c} we need to replan for the CAVs in the control zone. At any time t^{c}, we check whether t^{c} is a replanning instance if there exits HDV–$k \in \mathcal{H}(t^{\mathrm{c}})$ such that $\hat{\tau}_k(t^{\mathrm{c}}) \notin \mathrm{CI}_\zeta(\tau_k(\tilde{t}))$, where $\mathrm{CI}_\zeta(\cdot)$ denotes the $\zeta.100\%$ confidence interval of BLR prediction with $\zeta \in (0,1)$, and $\tilde{t}_k$ is the time that the last prediction for τ_k is stored.

Definition 3 implies that replanning is activated at time t^{c} if there is an HDV, e.g., HDV–k, whose actual time shift at t^{c} is outside the $\zeta.100\%$ confidence interval of the last stored prediction. The time that the last prediction for τ_k is stored can be either the entry time of HDV–k or the previous replanning instance. Once replanning is activated, we retrain the BLR model, update the trajectory and merging time predictions for the HDVs, and resolve Problem 3 given new initial conditions for some specific CAVs. The set of CAVs that need replanning is given in the following definition.

Definition 4: At a replanning instant t^{c}, let

$$\mathcal{H}'\left(t^{\mathrm{c}}\right) := \left\{k \in \mathcal{H}\left(t^{\mathrm{c}}\right) \mid \hat{\tau}_k\left(t^{\mathrm{c}}\right) \notin \mathrm{CI}_\zeta\left(\tau_k\left(\tilde{t}\right)\right)\right\}$$

be set of all HDVs that violate the condition $\hat{\tau}_k(t^{\mathrm{c}}) \in \mathrm{CI}_\zeta(\tau_k(\tilde{t}))$. Let HDV–$j$ be the HDV with the minimum predicted merging time in $\mathcal{H}'(t^{\mathrm{c}})$, i.e., $\mu_{t_j^{\mathrm{m}}} \leq \mu_{t_k^{\mathrm{m}}}$, $\forall k \in \mathcal{H}'(t^{\mathrm{c}})$. The set of CAVs that need replanning is determined as follows:

$$\begin{aligned}\mathcal{A}'\left(t^{\mathrm{c}}\right) := &\left\{i \in \mathcal{A}\left(t^{\mathrm{c}}\right) \cap \mathcal{R}_{j,\mathrm{S}}\left(t^{\mathrm{c}}\right) \mid t_i^0 > t_j^0\right\}\\ &\cup \left\{i \in \mathcal{A}\left(t^{\mathrm{c}}\right) \cap \mathcal{R}_{j,\mathrm{N}}\left(t^{\mathrm{c}}\right) \mid t_i^{\mathrm{m}} > \mu_{t_j^{\mathrm{m}}}-\rho_l\right\}\end{aligned} \tag{47}$$

where t_i^{m} is the planned merging time for CAV–i.
Definition 4 means that we replan for CAV–i either if: 1) CAV–i travels on the same road to HDV–j and enters the control zone after HDV–j or 2) CAV–i travels on the neighboring road to HDV–j and the planned merging time is greater than $\mu_{t_j^{\mathrm{m}}}-\rho_l$. The stochastic time-optimal control problem at any time t^{c} when a replanning event is activated can be given as follows.

Problem 4 (Stochastic Replanning in the Control Zone): At the time t^{c} with an replanning event, CAV–$i \in \mathcal{A}'(t^{\mathrm{c}})$ solves the following time-optimal control problem:

$$\underset{t_i^{\mathrm{f}} \in \mathcal{T}_i(t^{\mathrm{c}})}{\text{minimize}} \quad t_i^{\mathrm{f}}$$

subject to:

$$\begin{aligned}&(2),\ (3),\ (8),\\ &(40),\ \forall k \in \mathcal{R}_{i,\mathrm{N}}\left(t^{\mathrm{c}}\right),\\ &(41),\ k=\max\left\{j \in \mathcal{R}_{i,\mathrm{S}}\left(t^{\mathrm{c}}\right) \mid j<i\right\},\\ &(42),\ k=\max\left\{j \in \mathcal{R}_{i,\mathrm{N}}\left(t^{\mathrm{c}}\right) \mid t_j^{\mathrm{m}}<t_i^{\mathrm{m}}\right\},\end{aligned}$$

given:

$$\begin{aligned}&p_i\left(t^{\mathrm{c}}\right),\ v_i\left(t^{\mathrm{c}}\right),\\ &p_i\left(t_i^{\mathrm{f}}\right)=p^{\mathrm{f}},\ u_i\left(t_i^{\mathrm{f}}\right)=0.\end{aligned} \tag{48}$$

Thus, the replanning mechanism is summarized in Algorithm 1.

V. Simulation Results

In this section, we demonstrate the control performance of the proposed framework by numerical simulations.

A. Simulation Setup

For our simulation, we used PTV Vissim [82], which is a commercial software for simulating microscopic multimodal traffic flow. PTV Vissim provides a human-driven psycho-physical perception model created by Wiedemann [83]. To emulate the behavior of human drivers in a signal-free merging scenario, we leveraged the network object called "conflict areas" of the software where we assigned undetermined priority for the vehicles moving on two roadways. In the simulation, we considered a merging scenario with a buffer

Algorithm 1 Replanning Mechanism at Time t^{c}

Require: t^{c}, ζ, $\tilde{t}_k$, $\forall k \in \mathcal{H}(t^{\mathrm{c}})$
`Replan` $\leftarrow$ `False`
for $k \in \mathcal{H}(t^{\mathrm{c}})$ **do**
  Compute $\hat{\tau}_k(t^{\mathrm{c}})$
  if $t^{\mathrm{c}} = t_k^0$ **then**
    $\tilde{t}_k \leftarrow t^{\mathrm{c}}$
    Train $\mathcal{B}_k$
    Compute and store $\mu_{\tau_k}(\tilde{t}_k), \sigma^2_{\tau_k}(\tilde{t}_k)$
    Predict t_k^{m} and $\boldsymbol{\phi}_k$ using (35) and (30)/(33)
  else if $\hat{\tau}_k(t^{\mathrm{c}}) \notin \mathrm{CI}_\zeta(\tau_k(\tilde{t}_k))$ or `Replan` $=$ `True` **then**
    $\tilde{t}_k \leftarrow t^{\mathrm{c}}$
    Retrain $\mathcal{B}_k$
    Compute and store $\mu_{\tau_k}(\tilde{t}_k), \sigma^2_{\tau_k}(\tilde{t}_k)$
    Predict t_k^{m} and $\boldsymbol{\phi}_k$ using (35) and (30)/(33)
    `Replan` $\leftarrow$ `True`
Construct $\mathcal{A}'(t^{\mathrm{c}})$ using Definition 4
for $i \in \mathcal{A}(t^{\mathrm{c}})$ **do**
  if $t^{\mathrm{c}} = t_i^0$ **then**
    Solve Problem 3 given $p_i(t_i^0)$ and $v_i(t_i^0)$
  else if `Replan` and $i \in \mathcal{A}'(t^{\mathrm{c}})$ **then**
    Solve Problem 4 given $p_i(t^{\mathrm{c}})$ and $v_i(t^{\mathrm{c}})$

TABLE I
PARAMETERS OF THE TRAJECTORY PLANNING FRAMEWORK

Parameters	Values	Parameters	Values
$v_{\max}$	30.0 m/s	$v_{\min}$	3.0 m/s
$a_{\max}$	3.0 m/s^2	$a_{\min}$	-4.0 m/s^2
ρ_{l}	2.5 s	ρ_{r}	1.5 s
$d_{\min}$	10 m	H	20
ξ	0.95	ζ	0.8

zone of length 70 m, a control zone of length 430 m (350-m upstream and 80-m downstream of the merging point), and a virtual projection zone of length 100 m. The simulation environment in PTV Vissim is shown in Fig 5. In addition, the speed of congestion wave w in Newell's car-following model was chosen based on the traffic volume such that $3600\,w/n = 10$, where n denotes the traffic volume in vehicles per hour, which implies that the average standstill spacing is 10 m. The proposed trajectory planning framework was implemented using Python programming with the parameters in Table I. Videos and data of the simulations can be found at https://sites.google.com/cornell.edu/tcst-cav-mt.

Remark 3: The length of the control zone remarkably affects the overall performance of the proposed framework. If the control zone is too short, there may not be sufficient space for the CAVs to adjust their speed profiles without sharp braking, which could result in the backward propagation of traffic disruption. Through our simulation studies, the current control zone with a distance of 350 m from the entry to the merging point is approximately the minimum distance necessary to prevent traffic congestion in all examined simulations.

B. Results and Discussion

We conducted multiple simulations for three traffic volumes: 800, 1000, and 1200 vehicles per hour along with five different penetration rates: 0%, 40%, 60%, 80%, and 100%. In each simulation, we collected data for 500 s to compute the average travel time of the vehicles and reported the results in Table II.

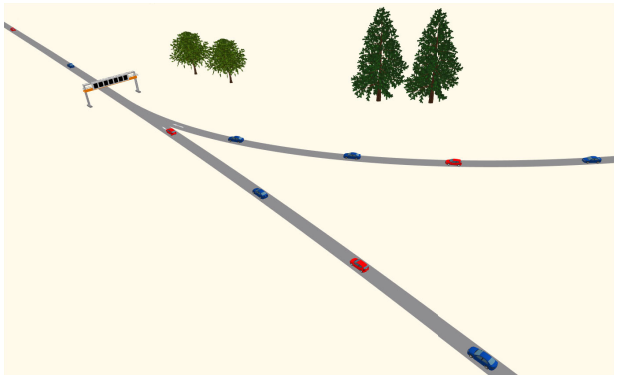

Fig. 5. Simulation environment in PTV Vissim.

TABLE II
AVERAGE TRAVEL TIME (IN S) UNDER DIFFERENT PENETRATION RATES AND TRAFFIC VOLUMES

Traffic volume \ Penetration rate	0%	40%	60%	80%	100%
800 (veh/h)	23.9	22.4	22.3	21.2	20.4
1000 (veh/h)	25.6	23.4	22.7	21.6	21.0
1200 (veh/h)	29.1	25.0	24.3	23.1	21.7

TABLE III
AVERAGE ACCELERATION (IN M/S^2) UNDER DIFFERENT PENETRATION RATES AND TRAFFIC VOLUMES

Traffic volume \ Penetration rate	0%	40%	60%	80%	100%
800 (veh/h)	0.92	0.86	0.76	0.65	0.49
1000 (veh/h)	0.90	0.89	0.80	0.71	0.56
1200 (veh/h)	0.91	0.87	0.75	0.70	0.56

As can be seen from Table II, at higher penetration rates, average travel times significantly improve compared to baseline traffic consisting solely of HDVs across all tested traffic volumes. For example, in the simulation with a high traffic volume of 1200 vehicles per hour, 40%, 60%, 80%, and 100% penetration rates can reduce average travel time by 14.1%, 16.5%, 20.6%, and 25.4%, respectively. The results also suggest that high penetration rates may be necessary for enhancing mixed traffic under high-volume conditions. Additionally, to quantify the motion smoothness of the vehicles, we compare the acceleration rates averaging among all the vehicles. For each vehicle i, the acceleration rate while traveling in the control zone is computed by the average acceleration from the entry time t_i^0 to the exit time t_i^{f} as follows:

$$\frac{1}{t_i^{\mathrm{f}} - t_i^0} \sqrt{\int_{\tau=t_i^0}^{t_i^{\mathrm{f}}} u_i^2(\tau)\, d\tau}. \tag{49}$$

We show the average acceleration rates in Table III. Overall, it can be observed that higher penetration rates of the CAVs result in smoother motion, which suggests better fuel consumption savings [84].

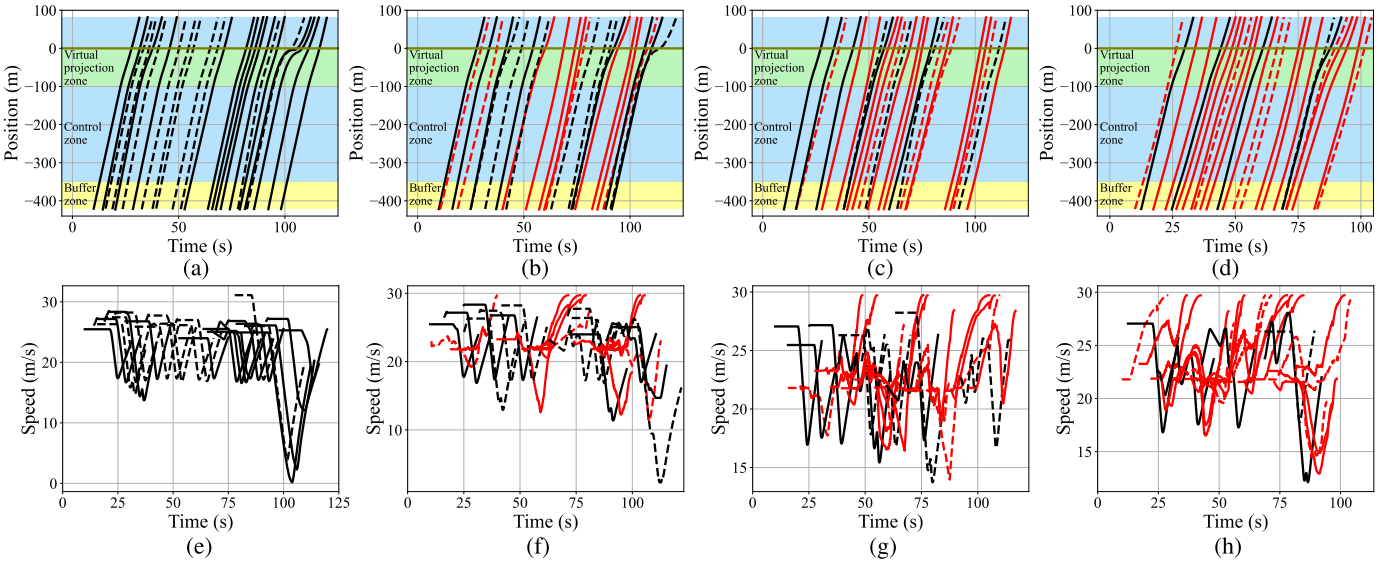

Fig. 6. Position trajectories and speed profiles of the first 25 vehicles in four simulations with different penetration rates. The trajectories for CAVs and HDVs are represented by red and black curves, respectively. Solid and dashed curves distinguish the vehicles moving on different roads. (a) and (e) 0% penetration rate. (b) and (f) 40% penetration rate. (c) and (g) 60% penetration rate. (d) and (h) 80% penetration rate.

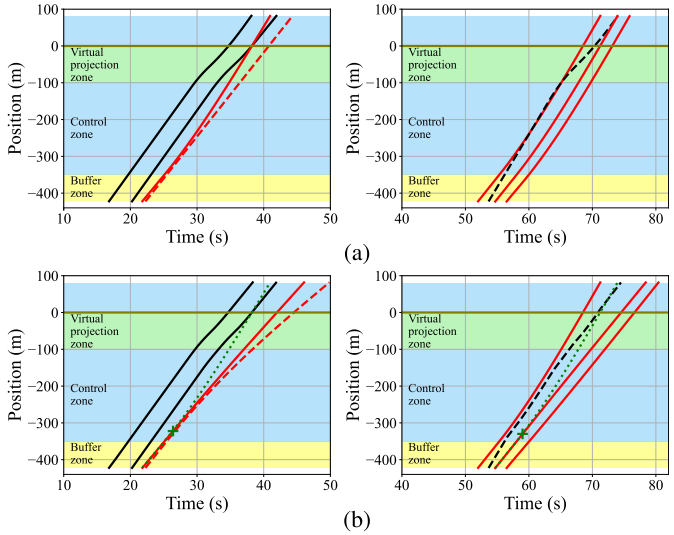

Fig. 7. Position trajectories for CAVs (red) and HDVs (black) in simulations (a) without and (b) with replanning. In the simulations without replanning, the safety constraints are activated for CAVs and HDVs entering from the same road (a-left) and from the neighboring road (a-right). Solid and dashed curves distinguish the vehicles moving on different roads. At the bottom, the green dotted curve represents the trajectory without replanning and a green cross marks the first replanning instance.

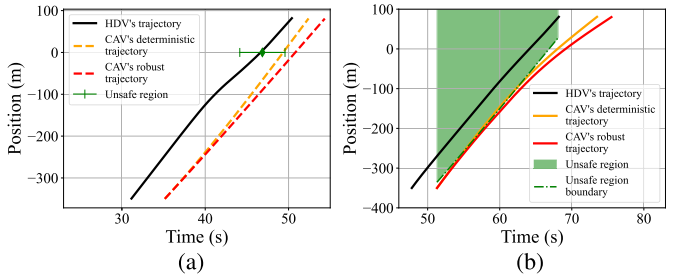

Fig. 8. Comparison between deterministic and robust trajectories for CAVs. Solid and dashed curves distinguish the vehicles moving on different roads. (a) Lateral constraint. (b) Rear-end constraint.

Next, we show the position trajectories and speed profiles of the first 25 vehicles in four simulations under 0%, 40%, 60%, and 80% penetration rates and the traffic volume of 1200 vehicles per hour in Fig. 6. The trajectories and speed profiles for 100% CAV coordination are similar to previous studies [85] and are thus omitted. Overall, the results show that under partial penetration rates, i.e., 40%, 60%, and 80%, the proposed framework guarantees safe coexistence between CAVs and HDVs [see Fig. 9(b)–(d)], and the corresponding simulation videos). Moreover, Fig. 6(e)–(h) suggest the potential benefits of coordination under increased CAV penetration rates in reducing traffic disruption. It is observed that HDVs generally exhibit more abrupt deceleration and acceleration compared to CAVs.

To better illustrate the advantages of the replanning mechanism, we show in Fig. 7 the position trajectories of some vehicles in the simulation with 60% penetration rate where without replanning the safety constraints are violated. The top panels of Fig. 7 reveal that the optimal trajectory of the CAVs, derived at the entry of the control zone, may cause a collision with either the preceding HDV or the HDV entering from the neighboring road due to the discrepancy between the HDV's predicted trajectory and the actual trajectory. On the other hand, the bottom panels demonstrate that with the proposed replanning mechanism, the CAVs can detect the changes in human driving behavior and replan a new trajectory to avoid collisions with the HDVs.

Safe maneuvers for CAVs can be further enhanced by using probabilistic constraints. In Fig. 8, we show the deterministic and robust trajectories derived at the control zone entry for particular CAVs in two simulations. For comparison purposes, we do not consider replanning in those simulations. In the first simulation [Fig. 8(a)], we define the unsafe region for merging time that is determined by values at which the tightened lateral constraint (44) is violated. Likewise, in the second simulation

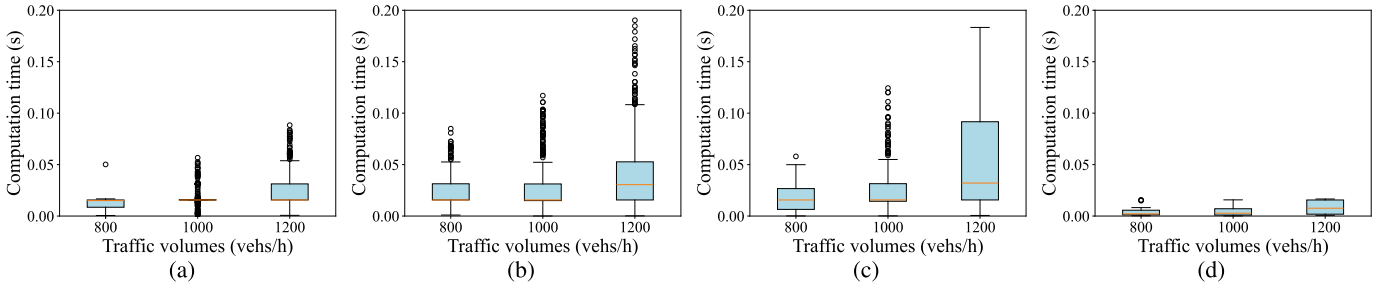

Fig. 9. Boxplots of computation time of the proposed algorithm under different traffic volumes and penetration rates. (a) 40% penetration rate. (b) 60% penetration rate. (c) 80% penetration rate. (d) 100% penetration rate.

[Fig. 8(b)], from the distribution of the time-shift prediction, we compute the unsafe region where the tightened rear-end constraint (45) is violated. In both cases, the robust trajectory can ensure that the CAV's trajectory and merging time do not invade the unsafe regions. Conversely, the deterministic trajectory violates the unsafe regions and may result in slightly more aggressive behavior. Note that the cautiousness of the stochastic planning framework can be adjusted by changing the probability of constraint satisfaction.

To evaluate the real-time practicality of the proposed framework, we collect the computation time at each planning and replanning instant for all the simulations performed on an Alienware computer with a 13th Gen Intel Core i9 CPU and 64-GB RAM, and show the statistical boxplots in Fig. 9. The computation time is the total time needed to learn the human driving model and solve the stochastic time-optimal control problem. The results show that the proposed framework generally takes a longer time to compute as the traffic volumes increase. Under a high traffic volume of 1200 vehicles per hour and partial penetration, the proposed framework takes no longer than 0.2 s per time step, with the third quantile being less than 0.1 s, which is reasonably good for real-time applications. Compared to the computation time under the full penetration rate, that under partial penetration is significantly higher. This is expected due to the computation required for BLR and the more frequent activation of replanning.

VI. Conclusion

In this article, we presented a trajectory planning framework that is safe, efficient, robust, and real-time practical for CAVs in mixed-traffic merging scenarios. We proposed a data-driven Newell's car-following model in which the time shift is calibrated online using BLR to model human driving behavior, and the virtual projection technique is used to capture the lateral interaction. We applied the data-driven Newell's car-following model to predict the trajectories and merging times of HDVs and quantified the prediction uncertainties used for probabilistic constraints in the stochastic time-optimal control problem. We developed a replanning mechanism to activate resolving the stochastic time-optimal control problem for CAVs if the last stored predictions are not sufficiently accurate compared to the actual observations. The results from simulations validate that our proposed framework can ensure safe maneuvers for CAVs among HDVs under different penetration rates and multiple traffic volumes. Moreover, the simulation results show that under higher penetration rates, two metrics, including average travel time and average acceleration rates of the vehicles, can be improved to some extent.

Several research directions can be considered in our future work. First, we will focus on extending the framework to consider more challenging scenarios such as multilane merges and intersections. Additionally, since the interaction between CAVs and HDVs becomes more complex and the coordination framework's efficiency diminishes given high traffic volumes, the ideas from optimal routing [86], [87] can be combined to control the traffic flow. Finally, we plan to validate the proposed framework in an experimental robotic testbed where human participants can drive robotic vehicles to constitute realistic mixed traffic [88].

Appendix
Proof of Lemma 1

Proof: Note that $\lambda_k \sim \mathcal{N}(\lambda_k, \sigma_{\tau_k}^2)$ where $\lambda_k = t - \mu_{\tau_k}$. From Newell's car-following model, we have

$$\begin{aligned} p_k(t) &= p_j(t-\tau_k(t)) - w\tau_k \\ &= \phi_{j,3}\lambda_k^3 + \phi_{j,2}\lambda_k^2 + \big(\phi_{j,1}+w\big)\lambda_k + \big(\phi_{j,0} - wt\big). \end{aligned} \tag{50}$$

The predicted mean of $p_k(t)$ can be found by taking the expectation of (50), i.e.,

$$\mathbb{E}\big[p_k(t)\big] = \mathbb{E}\big[\phi_{j,3}\lambda_k^3 + \phi_{j,2}\lambda_k^2 + \big(\phi_{j,1}+w\big)\lambda_k + \big(\phi_{j,0} - wt\big)\big]. \tag{51}$$

From the linearity of expectation, we have

$$\begin{aligned} \mathbb{E}\big[p_k(t)\big] = \phi_{j,3}\mathbb{E}\big[\lambda_k^3\big] + \phi_{j,2}\mathbb{E}\big[\lambda_k^2\big] + \big(\phi_{j,1}+w\big)\mathbb{E}[\lambda_k] \\ + \big(\phi_{j,0} - wt\big) \end{aligned} \tag{52}$$

where $\mathbb{E}[\lambda_k^n]$ denotes the nth moment of random variable $\lambda_k \sim \mathcal{N}(\lambda_k, \sigma_{\tau_k}^2)$. The nth moment of random variable λ_k can be obtained by evaluating the nth derivative of moment-generating function M_λ with respect to the slack variable τ and setting τ equal to zero, namely, $\mathbb{E}[\lambda_k^n] = \dfrac{d^n}{d\tau^n} M_\lambda(\tau)\,|_{\tau=0}$. The moment-generating function of random variable λ_k which is taken from a normal distribution is given by $M_e(\tau) = \exp(\tau\lambda_k + \dfrac{1}{2}\sigma_{\tau_k}^2\tau^2)$, where λ_k and $\sigma_{\tau_k}^2$ denote the mean and variance of the random variable, respectively. Following the above process, the first, second, and third moments of λ_k are derived as follows:

$$\mathbb{E}\big[\lambda_k^3\big] = \lambda_k^3 + 3\lambda_k\sigma_{\tau_k}^2 \tag{53}$$

$$\mathbb{E}\left[\lambda_k^2\right] = \lambda_k^2 + \sigma_{\tau_k}^2 \tag{54}$$

$$\mathbb{E}[\lambda_k] = \lambda_k. \tag{55}$$

Substituting (53)–(55) in (52), we get the the predicted mean of $p_k(t)$ as derived in (28). To find variance of $p_k(t)$, we employ $\sigma_{p_k}^2(t) = \mathbb{E}[p_k(t)^2] - \mathbb{E}[p_k(t)]^2$. The computation of the second term, $\mathbb{E}[p_k(t)]^2$, can be obtained by squaring (28). However, to derive the first term, $\mathbb{E}[p_k(t)^2]$, it is necessary first to compute $p_k(t)^2$, and afterward take its expectation. Utilizing (50), we have

$$p_k(t)^2 = \left(\phi_{j,3}\lambda_k^3 + \phi_{j,2}\lambda_k^2 + \phi'_{j,1}\lambda_k + \phi'_{j,0}\right)^2 \tag{56}$$

where $\phi'_{j,1} = \phi_{j,1} + w$ and $\phi'_{j,0} = \phi_{j,0} - wt$. Expanding (56), we have

$$\begin{aligned} p_k(t)^2 &= \lambda_k^6 \,{\phi_{j,3}}^2 + 2\,\lambda_k^5\,\phi_{j,2}\,\phi_{j,3} + 2\,\lambda_k^4\,\phi'_{j,1}\,\phi_{j,3} + \lambda_k^4\,{\phi_{j,2}}^2 \\ &\quad + 2\,\lambda_k^3\,\phi'_{j,0}\,\phi_{j,3} + 2\,\lambda_k^3\,\phi'_{j,1}\,\phi_{j,2} + 2\,\lambda_k^2\,\phi'_{j,0}\,\phi_{j,2} + \lambda_k^2\,{\phi'_{j,1}}^2 \\ &\quad + 2\,\lambda_k\,\phi'_{j,0}\,\phi'_{j,1} + {\phi'_{j,0}}^2. \end{aligned} \tag{57}$$

To compute the expectation of (57), we first need to derive fourth, fifth, and sixth moments of random variable λ_k as

$$\mathbb{E}\left[\lambda_k^6\right] = \lambda_k^6 + 15\lambda_k^4\,\sigma_{\tau_k}^2 + 45\,\lambda_k^2\,\sigma_{\tau_k}^4 + 15\,\sigma_{\tau_k}^6 \tag{58}$$

$$\mathbb{E}\left[\lambda_k^5\right] = \lambda_k^5 + 10\,\lambda_k^3\,\sigma_{\tau_k}^2 + 15\,\lambda_k\,\sigma_{\tau_k}^4 \tag{59}$$

$$\mathbb{E}\left[\lambda_k^4\right] = \lambda_k^4 + 6\lambda_k^2\sigma_{\tau_k}^2 + 3\sigma_{\tau_k}^4. \tag{60}$$

Next, we can derive the second moment of random variable $p_k(t)$, i.e., $\mathbb{E}[p_k(t)^2]$, by taking the expectation of (57) using the linearity of expectation and (53)–(55) and (58)–(60). Substituting the results in $\sigma_{p_k}^2(t) = \mathbb{E}[p_k(t)^2] - \mathbb{E}[p_k(t)]^2$, and performing some simple algebraic manipulations, we obtain (29). The derivation of $\boldsymbol{\phi}_k$ in (30) results from equating the coefficients of two polynomials in the left-hand and right-hand sides of (28), and the proof is complete. □

ACKNOWLEDGMENT

The authors would like to thank Dr. Ehsan Moradi-Pari at Honda Research Institute USA, Inc., Ann Arbor, MI, USA, for his valuable feedback on this article.

REFERENCES

[1] J. Rios-Torres and A. A. Malikopoulos, "Impact of partial penetrations of connected and automated vehicles on fuel consumption and traffic flow," *IEEE Trans. Intell. Vehicles*, vol. 3, no. 4, pp. 453–462, Dec. 2018.

[2] Y. Zhang and C. G. Cassandras, "An impact study of integrating connected automated vehicles with conventional traffic," *Annu. Rev. Control*, vol. 48, pp. 347–356, Jan. 2019.

[3] J. Ding, H. Peng, Y. Zhang, and L. Li, "Penetration effect of connected and automated vehicles on cooperative on-ramp merging," *IET Intell. Transport Syst.*, vol. 14, no. 1, pp. 56–64, 2020.

[4] A. A. Malikopoulos, L. Beaver, and I. V. Chremos, "Optimal time trajectory and coordination for connected and automated vehicles," *Automatica*, vol. 125, Mar. 2021, Art. no. 109469.

[5] A. A. Malikopoulos, C. G. Cassandras, and Y. J. Zhang, "A decentralized energy-optimal control framework for connected automated vehicles at signal-free intersections," *Automatica*, vol. 93, pp. 244–256, Jul. 2018.

[6] B. Chalaki and A. A. Malikopoulos, "Time-optimal coordination for connected and automated vehicles at adjacent intersections," *IEEE Trans. Intell. Transp. Syst.*, vol. 23, no. 8, pp. 13330–13345, Aug. 2022.

[7] B. Chalaki and A. A. Malikopoulos, "Optimal control of connected and automated vehicles at multiple adjacent intersections," *IEEE Trans. Control Syst. Technol.*, vol. 30, no. 3, pp. 972–984, May 2022.

[8] W. Xiao and C. G. Cassandras, "Decentralized optimal merging control for connected and automated vehicles with safety constraint guarantees," *Automatica*, vol. 123, Jan. 2021, Art. no. 109333.

[9] K. Xu, C. G. Cassandras, and W. Xiao, "Decentralized time and energy-optimal control of connected and automated vehicles in a roundabout with safety and comfort guarantees," *IEEE Trans. Intell. Transp. Syst.*, vol. 24, no. 1, pp. 657–672, Jan. 2023.

[10] R. Hult, M. Zanon, S. Gros, and P. Falcone, "Optimal coordination of automated vehicles at intersections: Theory and experiments," *IEEE Trans. Control Syst. Technol.*, vol. 27, no. 6, pp. 2510–2525, Nov. 2019.

[11] M. Kloock, P. Scheffe, S. Marquardt, J. Maczijewski, B. Alrifaee, and S. Kowalewski, "Distributed model predictive intersection control of multiple vehicles," in *Proc. IEEE Intell. Transp. Syst. Conf. (ITSC)*, Oct. 2019, pp. 1735–1740.

[12] A. Katriniok, B. Rosarius, and P. Mähönen, "Fully distributed model predictive control of connected automated vehicles in intersections: Theory and vehicle experiments," *IEEE Trans. Intell. Transp. Syst.*, vol. 23, no. 10, pp. 18288–18300, Oct. 2022.

[13] B. Chalaki et al., "Zero-shot autonomous vehicle policy transfer: From simulation to real-world via adversarial learning," in *Proc. IEEE 16th Int. Conf. Control Autom. (ICCA)*, Oct. 2020, pp. 35–40.

[14] S. K. Sumanth Nakka, B. Chalaki, and A. A. Malikopoulos, "A multi-agent deep reinforcement learning coordination framework for connected and automated vehicles at merging roadways," in *Proc. Amer. Control Conf. (ACC)*, Jun. 2022, pp. 3297–3302.

[15] E. Zhang, R. Zhang, and N. Masoud, "Predictive trajectory planning for autonomous vehicles at intersections using reinforcement learning," *Transp. Res. C, Emerg. Technol.*, vol. 149, Apr. 2023, Art. no. 104063.

[16] A. Katriniok, "Towards learning-based control of connected and automated vehicles: Challenges and perspectives," in *AI-Enabled Technologies for Autonomous and Connected Vehicles*. Cham, Switzerland: Springer, 2023, pp. 417–439.

[17] J. Rios-Torres and A. A. Malikopoulos, "A survey on the coordination of connected and automated vehicles at intersections and merging at highway on-ramps," *IEEE Trans. Intell. Transp. Syst.*, vol. 18, no. 5, pp. 1066–1077, May 2017.

[18] J. Guanetti, Y. Kim, and F. Borrelli, "Control of connected and automated vehicles: State of the art and future challenges," *Annu. Rev. Control*, vol. 45, pp. 18–40, Mar. 2018.

[19] T. Ersal et al., "Connected and automated road vehicles: State of the art and future challenges," *Vehicle Syst. Dyn.*, vol. 58, no. 5, pp. 672–704, May 2020.

[20] A. Alessandrini, A. Campagna, P. D. Site, F. Filippi, and L. Persia, "Automated vehicles and the rethinking of mobility and cities," *Transp. Res. Proc.*, vol. 5, pp. 145–160, Jan. 2015.

[21] Y. Wang et al., "Ego-efficient lane changes of connected and automated vehicles with impacts on traffic flow," *Transp. Res. C, Emerg. Technol.*, vol. 138, May 2022, Art. no. 103478.

[22] H. Bellem, T. Schönenberg, J. F. Krems, and M. Schrauf, "Objective metrics of comfort: Developing a driving style for highly automated vehicles," *Transp. Res. F, Traffic Psychol. Behaviour*, vol. 41, pp. 45–54, Aug. 2016.

[23] L. Jin, M. Cicic, K. H. Johansson, and S. Amin, "Analysis and design of vehicle platooning operations on mixed-traffic highways," *IEEE Trans. Autom. Control*, vol. 66, no. 10, pp. 4715–4730, Oct. 2021.

[24] M. F. Ozkan and Y. Ma, "Socially compatible control design of automated vehicle in mixed traffic," *IEEE Control Syst. Lett.*, vol. 6, pp. 1730–1735, 2022.

[25] J. Wang, Y. Zheng, Q. Xu, and K. Li, "Data-driven predictive control for connected and autonomous vehicles in mixed traffic," in *Proc. Amer. Control Conf. (ACC)*, Jun. 2022, pp. 4739–4745.

[26] A. M. I. Mahbub and A. A. Malikopoulos, "A platoon formation framework in a mixed traffic environment," *IEEE Control Syst. Lett.*, vol. 6, pp. 1370–1375, 2022.

[27] A. M. I. Mahbub, V.-A. Le, and A. A. Malikopoulos, "A safety-prioritized receding horizon control framework for platoon formation in a mixed traffic environment," *Automatica*, vol. 155, Sep. 2023, Art. no. 111115.

[28] Z. Fu, A. R. Kreidieh, H. Wang, J. W. Lee, M. L. D. Monache, and A. M. Bayen, "Cooperative driving for speed harmonization in mixed-traffic environments," in *Proc. IEEE Intell. Vehicles Symp. (IV)*, Jun. 2023, pp. 1–8.

[29] M. Bouton, A. Nakhaei, K. Fujimura, and M. J. Kochenderfer, "Cooperation-aware reinforcement learning for merging in dense traffic," in *Proc. IEEE Intell. Transp. Syst. Conf. (ITSC)*, Oct. 2019, pp. 3441–3447.

[30] D. Chen et al., "Deep multi-agent reinforcement learning for highway on-ramp merging in mixed traffic," *IEEE Trans. Intell. Transp. Syst.*, vol. 24, no. 11, pp. 11623–11638, Nov. 2023.

[31] W. Zhou, D. Chen, J. Yan, Z. Li, H. Yin, and W. Ge, "Multi-agent reinforcement learning for cooperative lane changing of connected and autonomous vehicles in mixed traffic," *Auto. Intell. Syst.*, vol. 2, no. 1, p. 5, Dec. 2022.

[32] B. Toghi, R. Valiente, D. Sadigh, R. Pedarsani, and Y. P. Fallah, "Social coordination and altruism in autonomous driving," *IEEE Trans. Intell. Transp. Syst.*, vol. 23, no. 12, pp. 24791–24804, Dec. 2022.

[33] R. Valiente, B. Toghi, M. Razzaghpour, R. Pedarsani, and Y. P. Fallah, "Learning-based social coordination to improve safety and robustness of cooperative autonomous vehicles in mixed traffic," in *Machine Learning and Optimization Techniques for Automotive Cyber-Physical Systems*. Cham, Switzerland: Springer, 2023, pp. 671–707.

[34] S. Udatha, Y. Lyu, and J. Dolan, "Reinforcement learning with probabilistically safe control barrier functions for ramp merging," in *Proc. IEEE Int. Conf. Robot. Autom. (ICRA)*, May 2023, pp. 5625–5630.

[35] B. Brito, A. Agarwal, and J. Alonso-Mora, "Learning interaction-aware guidance for trajectory optimization in dense traffic scenarios," *IEEE Trans. Intell. Transp. Syst.*, vol. 23, no. 10, pp. 18808–18821, Oct. 2022.

[36] M. Kuderer, S. Gulati, and W. Burgard, "Learning driving styles for autonomous vehicles from demonstration," in *Proc. IEEE Int. Conf. Robot. Autom. (ICRA)*, May 2015, pp. 2641–2646.

[37] F. S. Acerbo, H. Van der Auweraer, and T. D. Son, "Safe and computational efficient imitation learning for autonomous vehicle driving," in *Proc. Amer. Control Conf. (ACC)*, Jul. 2020, pp. 647–652.

[38] J. F. Fisac, E. Bronstein, E. Stefansson, D. Sadigh, S. S. Sastry, and A. D. Dragan, "Hierarchical game-theoretic planning for autonomous vehicles," in *Proc. Int. Conf. Robot. Autom. (ICRA)*, May 2019, pp. 9590–9596.

[39] L. Wang, L. Sun, M. Tomizuka, and W. Zhan, "Socially-compatible behavior design of autonomous vehicles with verification on real human data," *IEEE Robot. Autom. Lett.*, vol. 6, no. 2, pp. 3421–3428, Apr. 2021.

[40] D. Sadigh, N. Landolfi, S. S. Sastry, S. A. Seshia, and A. D. Dragan, "Planning for cars that coordinate with people: Leveraging effects on human actions for planning and active information gathering over human internal state," *Auto. Robots*, vol. 42, no. 7, pp. 1405–1426, Oct. 2018.

[41] M. Liu, I. Kolmanovsky, H. E. Tseng, S. Huang, D. Filev, and A. Girard, "Potential game-based decision-making for autonomous driving," *IEEE Trans. Intell. Transp. Syst.*, 2023.

[42] B. Evens, M. Schuurmans, and P. Patrinos, "Learning MPC for interaction-aware autonomous driving: A game-theoretic approach," in *Proc. Eur. Control Conf. (ECC)*, Jul. 2022, pp. 34–39.

[43] W. Schwarting, A. Pierson, J. Alonso-Mora, S. Karaman, and D. Rus, "Social behavior for autonomous vehicles," *Proc. Nat. Acad. Sci. USA*, vol. 116, no. 50, pp. 24972–24978, 2019.

[44] X. Zhao, Y. Tian, and J. Sun, "Yield or rush? Social-preference-aware driving interaction modeling using game-theoretic framework," in *Proc. IEEE Int. Intell. Transp. Syst. Conf. (ITSC)*, Sep. 2021, pp. 453–459.

[45] H. Hu and J. F. Fisac, "Active uncertainty reduction for human–robot interaction: An implicit dual control approach," in *Proc. 15th Workshop Algorithmic Found. Robot.* Cham, Switzerland: Springer, 2023, pp. 385–401.

[46] S. H. Nair, V. Govindarajan, T. Lin, C. Meissen, H. E. Tseng, and F. Borrelli, "Stochastic MPC with multi-modal predictions for traffic intersections," in *Proc. IEEE 25th Int. Conf. Intell. Transp. Syst. (ITSC)*, Oct. 2022, pp. 635–640.

[47] M. Schuurmans, A. Katriniok, C. Meissen, H. E. Tseng, and P. Patrinos, "Safe, learning-based MPC for highway driving under lane-change uncertainty: A distributionally robust approach," *Artif. Intell.*, vol. 320, Jul. 2023, Art. no. 103920.

[48] S. Bae et al., "Lane-change in dense traffic with model predictive control and neural networks," *IEEE Trans. Control Syst. Technol.*, vol. 31, no. 2, pp. 646–659, Mar. 2023.

[49] P. Gupta, D. Isele, D. Lee, and S. Bae, "Interaction-aware trajectory planning for autonomous vehicles with analytic integration of neural networks into model predictive control," in *Proc. IEEE Int. Conf. Robot. Autom. (ICRA)*, May 2023, pp. 7794–7800.

[50] N. Venkatesh, V.-A. Le, A. Dave, and A. A. Malikopoulos, "Connected and automated vehicles in mixed-traffic: Learning human driver behavior for effective on-ramp merging," in *Proc. 62nd IEEE Conf. Decis. Control (CDC)*, Dec. 2023, pp. 92–97.

[51] V.-A. Le and A. A. Malikopoulos, "Optimal weight adaptation of model predictive control for connected and automated vehicles in mixed traffic with Bayesian optimization," in *Proc. Amer. Control Conf. (ACC)*, May 2023, pp. 1183–1188.

[52] V.-A. Le and A. A. Malikopoulos, "A cooperative optimal control framework for connected and automated vehicles in mixed traffic using social value orientation," in *Proc. IEEE 61st Conf. Decis. Control (CDC)*, Dec. 2022, pp. 6272–6277.

[53] E. Sabouni, H. M. S. Ahmad, C. G. Cassandras, and W. Li, "Merging control in mixed traffic with safety guarantees: A safe sequencing policy with optimal motion control," in *Proc. IEEE 26th Int. Conf. Intell. Transp. Syst. (ITSC)*, Sep. 2023, pp. 4260–4265.

[54] A. Li, A. S. C. Armijos, and C. G. Cassandras, "Cooperative lane changing in mixed traffic can be robust to human driver behavior," in *Proc. 62nd IEEE Conf. Decis. Control (CDC)*, Dec. 2023, pp. 5123–5128.

[55] B. Chalaki et al., "Minimally disruptive cooperative lane-change maneuvers," *IEEE Control Syst. Lett.*, vol. 7, pp. 1766–1771, 2023.

[56] Z. Yan and C. Wu, "Reinforcement learning for mixed autonomy intersections," in *Proc. IEEE Int. Intell. Transp. Syst. Conf. (ITSC)*, Sep. 2021, pp. 2089–2094.

[57] B. Peng, M. F. Keskin, B. Kulcsár, and H. Wymeersch, "Connected autonomous vehicles for improving mixed traffic efficiency in unsignalized intersections with deep reinforcement learning," *Commun. Transp. Res.*, vol. 1, Dec. 2021, Art. no. 100017.

[58] M. Faris, P. Falcone, and J. Sjöberg, "Optimization-based coordination of mixed traffic at unsignalized intersections based on platooning strategy," in *Proc. IEEE Intell. Vehicles Symp. (IV)*, Jun. 2022, pp. 977–983.

[59] N. Buckman, A. Pierson, W. Schwarting, S. Karaman, and D. Rus, "Sharing is caring: Socially-compliant autonomous intersection negotiation," in *Proc. IEEE/RSJ Int. Conf. Intell. Robots Syst. (IROS)*, Nov. 2019, pp. 6136–6143.

[60] A. Ghosh and T. Parisini, "Traffic control in a mixed autonomy scenario at urban intersections: An optimal control approach," *IEEE Trans. Intell. Transp. Syst.*, vol. 23, no. 10, pp. 17325–17341, Oct. 2022.

[61] N. Suriyarachchi, R. Quirynen, J. S. Baras, and S. Di Cairano, "Optimization-based coordination and control of traffic lights and mixed traffic in multi-intersection environments," in *Proc. Amer. Control Conf. (ACC)*, May 2023, pp. 3162–3168.

[62] H. Liu, W. Zhuang, G. Yin, Z. Li, and D. Cao, "Safety-critical and flexible cooperative on-ramp merging control of connected and automated vehicles in mixed traffic," *IEEE Trans. Intell. Transp. Syst.*, vol. 24, no. 3, pp. 2920–2934, Mar. 2023.

[63] V.-A. Le, H. M. Wang, G. Orosz, and A. A. Malikopoulos, "Coordination for connected automated vehicles at merging roadways in mixed traffic environment," in *Proc. 62nd IEEE Conf. Decis. Control (CDC)*, Dec. 2023, pp. 4150–4155.

[64] G. F. Newell, "A simplified car-following theory: A lower order model," *Transp. Res. B, Methodol.*, vol. 36, no. 3, pp. 195–205, Mar. 2002.

[65] B. Chalaki and A. A. Malikopoulos, "Robust learning-based trajectory planning for emerging mobility systems," in *Proc. Amer. Control Conf. (ACC)*, Jun. 2022, pp. 2154–2159.

[66] A. E. Bryson and Y. C. Ho, *Applied Optimal Control: Optimization, Estimation and Control*. Boca Raton, FL, USA: CRC Press, 1975.

[67] G. Cardano, T. R. Witmer, and O. Ore, *The Rules of Algebra: Ars Magna*, vol. 685. New York, NY, USA: Courier Corporation, 2007.

[68] B. Chalaki, L. E. Beaver, and A. A. Malikopoulos, "Experimental validation of a real-time optimal controller for coordination of CAVs in a multi-lane roundabout," in *Proc. IEEE Intell. Vehicles Symp. (IV)*, Oct. 2020, pp. 504–509.

[69] C. M. Bishop and N. M. Nasrabadi, *Pattern Recognition and Machine Learning*, vol. 4. Berlin, Germany: Springer, 2006.

[70] G. Li, Y. Jiao, V. L. Knoop, S. C. Calvert, and J. Van Lint, "Large car-following data based on Lyft level-5 open dataset: Following autonomous vehicles vs. human-driven vehicles," in *Proc. IEEE 26th Int. Conf. Intell. Transp. Syst. (ITSC)*, May 2023, pp. 5818–5823.

[71] S. Wong, L. Jiang, R. Walters, T. G. Molnár, G. Orosz, and R. Yu, "Traffic forecasting using vehicle-to-vehicle communication," in *Proc. 3rd Conf. Learn. Dyn. Control*, vol. 211, 2021, pp. 917–929.

[72] T. G. Molnar et al., "On-board traffic prediction for connected vehicles: Implementation and experiments on highways," in *Proc. Amer. Control Conf. (ACC)*, Jun. 2022, pp. 1036–1041.

[73] D. Holley, J. D'sa, H. N. Mahjoub, G. Ali, B. Chalaki, and E. Moradi-Pari, "MR-IDM-Merge reactive intelligent driver model: Towards enhancing laterally aware car-following models," in *Proc. IEEE 26th Int. Conf. Intell. Transp. Syst. (ITSC)*, Sep. 2023, pp. 1460–1467.

[74] K. Kreutz and J. Eggert, "Analysis of the generalized intelligent driver model (GIDM) for merging situations," in *Proc. IEEE Intell. Vehicles Symp. (IV)*, Jul. 2021, pp. 34–41.

[75] Y. Guo, Q. Sun, R. Fu, and C. Wang, "Improved car-following strategy based on merging behavior prediction of adjacent vehicle from naturalistic driving data," *IEEE Access*, vol. 7, pp. 44258–44268, 2019.

[76] T. Brüdigam, M. Olbrich, D. Wollherr, and M. Leibold, "Stochastic model predictive control with a safety guarantee for automated driving," *IEEE Trans. Intell. Vehicles*, vol. 8, no. 1, pp. 22–36, Jan. 2023.

[77] T. Lew, R. Bonalli, and M. Pavone, "Chance-constrained sequential convex programming for robust trajectory optimization," in *Proc. Eur. Control Conf. (ECC)*, May 2020, pp. 1871–1878.

[78] J. Coulson, J. Lygeros, and F. Dörfler, "Distributionally robust chance constrained data-enabled predictive control," *IEEE Trans. Autom. Control*, vol. 67, no. 7, pp. 3289–3304, Jul. 2022.

[79] L. Hewing, J. Kabzan, and M. N. Zeilinger, "Cautious model predictive control using Gaussian process regression," *IEEE Trans. Control Syst. Technol.*, vol. 28, no. 6, pp. 2736–2743, Nov. 2020.

[80] T. X. Nghiem and C. N. Jones, "Data-driven demand response modeling and control of buildings with Gaussian processes," in *Proc. Amer. Control Conf. (ACC)*, Mar. 2017, pp. 2919–2924.

[81] J. Boedecker, J. T. Springenberg, J. Wulfing, and M. Riedmiller, "Approximate real-time optimal control based on sparse Gaussian process models," in *Proc. IEEE Symp. Adapt. Dyn. Program. Reinforcement Learn. (ADPRL)*, Dec. 2014, pp. 1–8.

[82] A. Evanson, "Connected autonomous vehicle (CAV) simulation using PTV vissim," in *Proc. Winter Simulation Conf. (WSC)*, Dec. 2017, p. 4420.

[83] R. Wiedemann, *Simulation Des Strassenverkehrsflusses*. Karlsruhe, Germany: Univ. Karlsruhe, Institut fur Verkehrswesen, 1974.

[84] A. A. Malikopoulos, D. N. Assanis, and P. Y. Papalambros, "Optimal engine calibration for individual driving styles," SAE Tech. Paper 2008-01-1367, 2008.

[85] A. M. I. Mahbub, A. A. Malikopoulos, and L. Zhao, "Decentralized optimal coordination of connected and automated vehicles for multiple traffic scenarios," *Automatica*, vol. 117, Jul. 2020, Art. no. 108958.

[86] H. Bang, B. Chalaki, and A. A. Malikopoulos, "Combined optimal routing and coordination of connected and automated vehicles," *IEEE Control Syst. Lett.*, vol. 6, pp. 2749–2754, 2022.

[87] H. Bang, A. Dave, and A. A. Malikopoulos, "Routing in mixed transportation systems for mobility equity," 2023, *arXiv:2309.03981*.

[88] B. Chalaki, L. E. Beaver, A. M. I. Mahbub, H. Bang, and A. A. Malikopoulos, "A research and educational robotic testbed for real-time control of emerging mobility systems: From theory to scaled experiments," *IEEE Control Syst.*, vol. 42, no. 6, pp. 20–34, Dec. 2022.

Viet-Anh Le (Student Member, IEEE) received the B.S. degree in automation and control engineering from Hanoi University of Science and Technology, Hanoi, Vietnam, in 2019, and the M.S. degree in informatics from Northern Arizona University, Flagstaff, AZ, USA, in 2021. He is currently pursuing the Ph.D. degree in mechanical engineering with an emphasis on robotics and control with the University of Delaware, Newark, DE, USA.

He joined Honda Research Institute USA, Inc., Ann Arbor, MI, USA, as a Research Intern, in 2023. He is also a Visiting (nondegree) Graduate Student of systems engineering with Cornell University, Ithaca, NY, USA. His research interests include learning-based control, model predictive control, distributed optimization, multiagent systems, and human–robot interaction, with a typical application in connected and automated vehicles.

Behdad Chalaki (Member, IEEE) received the B.S. degree in mechanical engineering from the University of Tehran, Tehran, Iran, in 2017, and the M.S. and Ph.D. degrees from the Department of Mechanical Engineering, University of Delaware, Newark, DE, USA, in 2021 and 2022, respectively.

His Ph.D. research concentrated on developing online decentralized control algorithms for coordinating connected and automated vehicles (CAVs) in diverse traffic scenarios, addressing uncertainties in motion planning. He is currently a Research Scientist with Honda Research Institute USA, Inc., Ann Arbor, MI, USA. His current research focuses on decision-making, motion planning, and control of multirobot systems coexisting with humans, utilizing techniques from artificial intelligence and optimal control.

Filippos N. Tzortzoglou (Student Member, IEEE) received the Diploma with an integrated M.S. degree in production engineering and management from the Technical University of Crete, Chania, Greece, in 2022. He is currently pursuing the Ph.D. degree with the Civil and Environmental Engineering Department, Cornell University, Ithaca, NY, USA.

In 2022, he joined the Mechanical Engineering Department, University of Delaware, Newark, DE, USA, as a Research and Teaching Assistant. He is currently working as an Intern with MathWorks, Natick, MA, USA. His research interests lie in the area of automatic control and machine learning, with applications in transportation and autonomous vehicles.

Mr. Tzortzoglou has received several fellowships from foundations across the USA and the National Research Foundation.

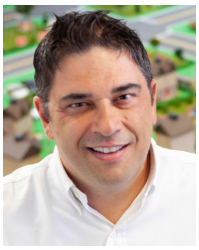

Andreas A. Malikopoulos (Senior Member, IEEE) received the Diploma degree in mechanical engineering from the National Technical University of Athens (NTUA), Athens, Greece, in 2000, and the M.S. and Ph.D. degrees in mechanical engineering from the University of Michigan, Ann Arbor, MI, USA, in 2004 and 2008, respectively.

From 2008 to 2010, he was a Senior Researcher with General Motors Global Research and Development, Oak Ridge National Laboratory (ORNL), Oak Ridge, TN, USA, where he was the Alvin M. Weinberg Fellow with the Energy and Transportation Science Division, from 2010 to 2017, and the Deputy Director of the Urban Dynamics Institute, from 2014 to 2017. From 2017 to 2023, he was the Terri Connor Kelly and John Kelly Career Development Professor with the Department of Mechanical Engineering, University of Delaware (UD), Newark, DE, USA, where he was the Founding Director of the Sociotechnical Systems Center, from 2019 to 2023. He is currently a Professor with the School of Civil and Environmental Engineering, Cornell University, Ithaca, NY, USA, and also the Director of the Information and Decision Science (IDS) Laboratory. His research spans several fields, including analysis, optimization, and control of cyber-physical systems (CPS); decentralized stochastic systems; stochastic scheduling and resource allocation; and learning in complex systems. His research aims to develop theories and data-driven system approaches at the intersection of learning and control for making CPS able to realize their optimal operation while interacting with their environment.

Dr. Malikopoulos was an Associate Editor of IEEE TRANSACTIONS ON INTELLIGENT VEHICLES and IEEE TRANSACTIONS ON INTELLIGENT TRANSPORTATION SYSTEMS, from 2017 to 2020. He is currently an Associate Editor of *Automatica* and IEEE TRANSACTIONS ON AUTOMATIC CONTROL, and a Senior Editor of IEEE TRANSACTIONS ON INTELLIGENT TRANSPORTATION SYSTEMS. He is a member of SIAM and AAAS, and a fellow of ASME.